Deep–Sea Research I 198 (2023) 104081

Contents lists available at ScienceDirect

Deep-Sea Research Part I

journal homepage: www.elsevier.com/locate/dsri

Seasonal and interannual variability of Mediterranean Sea overturning circulation

J.-M. Sayol [a,*], M. Marcos [b,c], D. Garcia-Garcia [a], I. Vigo [a]

[a] Department of Applied Mathematics, University of Alicante, Sant Vicent del Raspeig, Alicante, Spain
[b] Department of Physics, Universitat de les Illes Balears, Palma, Mallorca, Spain
[c] IMEDEA (UIB-CSIC), Esporles, Mallorca, Spain

ARTICLE INFO

Keywords:
Mediterranean sea
Overturning circulation
Deep convection
Water mass transformation
Seasonality
Interannual variability

ABSTRACT

The overturning streamfunction is a widely used metric to monitor ocean circulation changes in the North Atlantic Ocean. Analogously, it is known that an overturning circulation develops in the Mediterranean Sea, although substantially weaker and smaller than in the Atlantic. In this work we use monthly mean fields from a high-resolution ocean reanalysis (1/16° × 1/16°) to explore seasonal and interannual variability of Mediterranean Sea overturning circulation in depth and water mass parameter spaces (potential density, potential temperature, salinity) from 1987 to 2018 (both included). Results show a clear single zonal clockwise transport cell in all three spaces that extends from the Strait of Gibraltar to the Levantine Basin, in which water masses tend to densify as they move eastward. This densification is mainly controlled by salinity in the Eastern Mediterranean basin (EMED), while in the Western Mediterranean (WMED) both salinity and potential temperature variations should be taken into account. In contrast, the meridional overturning transport, much more complex, is able to better capture smaller-scale variations since it responds faster to perturbations in the circulation.

Seasonal variations in overturning transport are reflected in the size and strength of overturning cells in all spaces, being cells remarkably narrower in winter than in summer. Regarding interannual changes, we show that the meridional overturning transport in density space is significantly correlated with the North Atlantic Oscillation, the Mediterranean Oscillation Index and the Scandinavian pattern during wintertime in the WMED, and with the Eastern Atlantic and the East Atlantic–Western Russian in the EMED. The overturning metric in density space captures well the Eastern Mediterranean Transient, that occurred during years 1992–1996. Finally, we explore the usefulness of overturning metric to detect and track water mass changes associated to shorter scale events, using as example the strong deep convection events of years 2004–2006 in the Gulf of Lion, which marked the beginning of the Western Mediterranean Transition.

1. Introduction

The Atlantic component of the global overturning circulation, the Atlantic Meridional Overturning Circulation (AMOC), plays a fundamental role in the Earth's energy balance (e.g. Drijfhout, 2015; Liu et al., 2020). Several works have explored how the AMOC could be impacted under the ongoing global warming (e.g. Zhu et al., 2015; Boers, 2021). In response to those concerns and to bring some light on the physical mechanisms driving the changes in the AMOC, the scientific community fostered some initiatives to perform direct measurements of its state at key regions. Thus, its transport is being routinely measured in subtropical (26.5°N) and subpolar (~55°N) North Atlantic areas through both RAPID-MOCHA-WBTS and OSNAP research programs, which started in 2004 and 2014, respectively (Smeed et al., 2014; Lozier et al., 2019). In this regard, the most recent sixth assessment (AR6) IPCC report states that very likely the AMOC will decline during the 21st century (Fox-Kemper et al., 2021).

Analogously to the Atlantic Ocean, the Mediterranean Sea also has its own overturning circulation, although substantially weaker and on a shorter time scale (Zavatarelli and Mellor, 1995; Demirov and Pinardi, 2007; Pinardi et al., 2019). With a mean volume transport of around 1 Sv and time scales of up to a few years, numbers are comparably lower than the 15–30 Sv and the decades found for some pathways associated with the AMOC (Smeed et al., 2018; Lozier et al., 2019; Bower et al., 2019; Georgiou et al., 2021). Substantial changes in the Mediterranean Sea overturning are intimately related with the North Atlantic circulation in a bidirectional way, as some paleo and/or

* Corresponding author.
E-mail address: juanma.sayol@ua.es (J.-M. Sayol).

https://doi.org/10.1016/j.dsr.2023.104081
Received 8 December 2022; Received in revised form 29 May 2023; Accepted 2 June 2023
Available online 5 June 2023

modeling studies have reported (e.g. Aldama-Campino and Döös, 2020; Ayache et al., 2021). Therefore the Mediterranean Sea can be seen as a small "ocean lab" with a circulation easier to monitoring than in the North Atlantic, and at the same time useful to get new insights into AMOC variability due to its still remarkable complexity.

The Mediterranean Sea is a semi-enclosed concentration basin connected to the North Atlantic Ocean through the Strait of Gibraltar. Although initially its circulation was depicted by a three-layer circulation driven by cyclonic motions (Wüst, 1961), it was later recognized as an open thermohaline cell with two closed secondary cells (Lascaratos et al., 1999; Bergamasco and Malanotte-Rizzoli, 2010), one for each sub-basin (Western and Eastern Mediterranean Sea, respectively), separated by the Strait of Sicily. Recently, Pinardi et al. (2019) highlighted another secondary cell in the Eastern Mediterranean around the Rhodes region that extends up to deeper layers, thus depicting an even more complex view of the Mediterranean Sea circulation. The basin-scale cell is maintained by the input of surface colder and fresher Atlantic Water, which is transformed (becomes denser) as it recirculates along the basin due to both the excess of evaporation and winter cooling, to finally return into the Atlantic at deeper layers (Astraldi et al., 1999; Millot, 1999; Malanotte-Rizzoli et al., 1999). The cyclonic circulation separates heavier waters allocated in the center of the basin from lighter waters circulating along the periphery. This scenario results in a progressive slope of isopycnals towards the surface (Gascard, 1978). Western and Eastern Mediterranean sub-basins display different water mass properties, with more saline and warmer waters in the eastern basin. Water masses are subject to transformation as a consequence of the local conditions that control the regional basins, which contribute to produce new water mass classes. Additionally, straits and channels within the Mediterranean are choke points where water mass properties are exchanged (e.g., Heslop et al., 2012).

The enhanced ocean heat loss favors the formation of relatively cold intermediate and deep waters during winter in a few Mediterranean Sea regions (Wüst, 1961; Millot, 1999; Malanotte-Rizzoli et al., 1999). In the Western Mediterranean Sea, strong winter deep and intermediate convection events occur from time to time (Schröder et al., 2006; Schroeder et al., 2008). The formation of deep waters that occurs in the Gulf of Lion normally consists of three steps (e.g. Rhein, 1995; Houpert et al., 2016): (1) onset or preconditioning between October and the end of January that reduces stratification between Atlantic Water and Levantine Intermediate Water (AW and LIW, respectively, both indicated in Fig. 1); (2) a strong mixing with large vertical velocities that occurs along convection chimneys of about 1 km of diameter; (3) the transport of new waters away from the convection region by baroclinic eddies. These eddies develop at the border between stratified and well-mixed waters and have a size of 5–10 km. About 2–3 weeks later the convection region is restratified by eddies, and the new water properties have spread out of the convection region. Despite strong vertical velocities can be found in the interior near deep convection sites, net sinking is restricted to near-boundary areas (Waldman et al., 2018; Brüggemann and Katsman, 2019), as it occurs in large areas of the subpolar North Atlantic (Katsman et al., 2018; Sayol et al., 2019).

On the other hand, water densities in the Eastern Mediterranean Sea are higher and governed by salt enrichment, as a result of an excess of evaporation (Roether et al., 1996). There, dense water formation has been traditionally observed in the southern Adriatic Sea when surface waters, preconditioned by high salinity, become sufficiently dense by cooling. However, between the late 80's and the mid 90's, Adriatic waters got less saline and this deep water formation site switched to the Aegean Sea, which changed appreciably the deep distributions of all water mass properties in the Eastern Mediterranean (Lascaratos et al., 1999; Manca et al., 2006). This transition period, known as the Eastern Transient, has been the focus of many studies, although there exists now some consensus on the relevant role that play lateral salinity fluxes on the bimodal dynamics of LIW in the Ionian Sea (Klein et al., 1999), with associated changes in pathways and water mass properties (Hainbucher et al., 2006; Manca et al., 2006). Other effects that were mentioned as triggers of the Eastern Transient are an unusual heat loss (due to strong air–sea interactions or by a longer dry period with large net evaporation), the overlapping of decadal sub-basin salinity variations, or the retention of sediments by river damming, among other (Rohling and Bryden, 1992; Theocharis et al., 1999; Wu et al., 2000; Josey, 2003; Pisacane et al., 2006). At interannual scale, the North Atlantic Oscillation (NAO) and the Eastern Atlantic have been identified as important signals associated to changes in sea level, sea surface temperature, mean and extreme waves and water transport in several Mediterranean regions, especially during wintertime (Rixen et al., 2005; Vigo et al., 2011; Morales-Márquez et al., 2020; García-García et al., 2022). Also the East Atlantic–Western Russia pattern and the Scandinavian pattern affect the Eastern Mediterranean hydrological balance and hence the ocean transport (Krichak and Alpert, 2005). More recently, it has been pointed out the good correlation of the Mediterranean Oscillation Index (MOI) with changes in Mediterranean Sea thermohaline circulation, although the MOI is not totally independent from NAO (Criado-Aldeanueva and Soto-Navarro, 2020).

Water mass transformation and pathways are influenced by meso- and submesoscale processes such as gyres, coherent vortexes and fronts. The role of quasi-permanent gyres and eddies in the overturning circulation was recenty addressed by Pinardi et al. (2019) through using the residual overturning metric, in which the eddy and the mean overturning components were evaluated separately. They found an important role of diapycnal mixing induced by bottom friction in controlling the circulation in the basin, especially in the eastern sub-basin, where the Eastern Mediterranean Transient was studied from an overturning perspective. In this work we complement the work of Pinardi et al. (2019) by analyzing the seasonal and the inter-annual variability of Mediterranean Sea overturning in potential density, salinity and potential temperature spaces. This approach allows to characterize the overturning cell and its variations in terms of water mass properties since changes in potential temperature and/or salinity space might be reflected in potential density. Finally, we characterize overturning anomalies of water mass properties during the strong winter deep convection events occurred in the Western Mediterranean between 2004–2006. Those years marked the beginning of the Western Mediterranean Transition (WMT), known by a cooling and freshening of intermediate layers and a warming and a rise in salinity in the bottom layers (Zunino et al., 2012; Schroeder et al., 2016). After 2004–2006, other episodes of strong convection at intermediate layers have been reported in the Gulf of Lion for winters of 2013 and 2018 (Margirier et al., 2020).

The rest of the article is distributed as follows: in Section 2 model data and the overturning metrics are described; Section 3 characterizes the mean zonal and meridional overturning patterns; Section 4 describes the seasonal and interannual overturning signals; in Section 5 we study the deep convection events occurred in the Western Mediterranean Sea during years 2004–2006 with more detail from the perspective of overturning; finally, Section 6 provides a summary of main results and conclusions.

2. Data and methods

2.1. Ocean reanalysis

To derive overturning we employ a longer version of the Mediterranean Sea reanalysis used by Pinardi et al. (2019), which covered from 1987 to 2011. This eddy-resolving simulation was part of the catalog of products available at Copernicus Marine Environment Monitoring Service (Simoncelli et al., 2017) with code MEDSEA_REANALYSIS_PHYS_006_004, until its replacement by a higher vertical resolution product. The reanalysis is based on the Nucleus for European Modelling of the Ocean (NEMO) version 3.2 (Madec, 2008), and solves the primitive

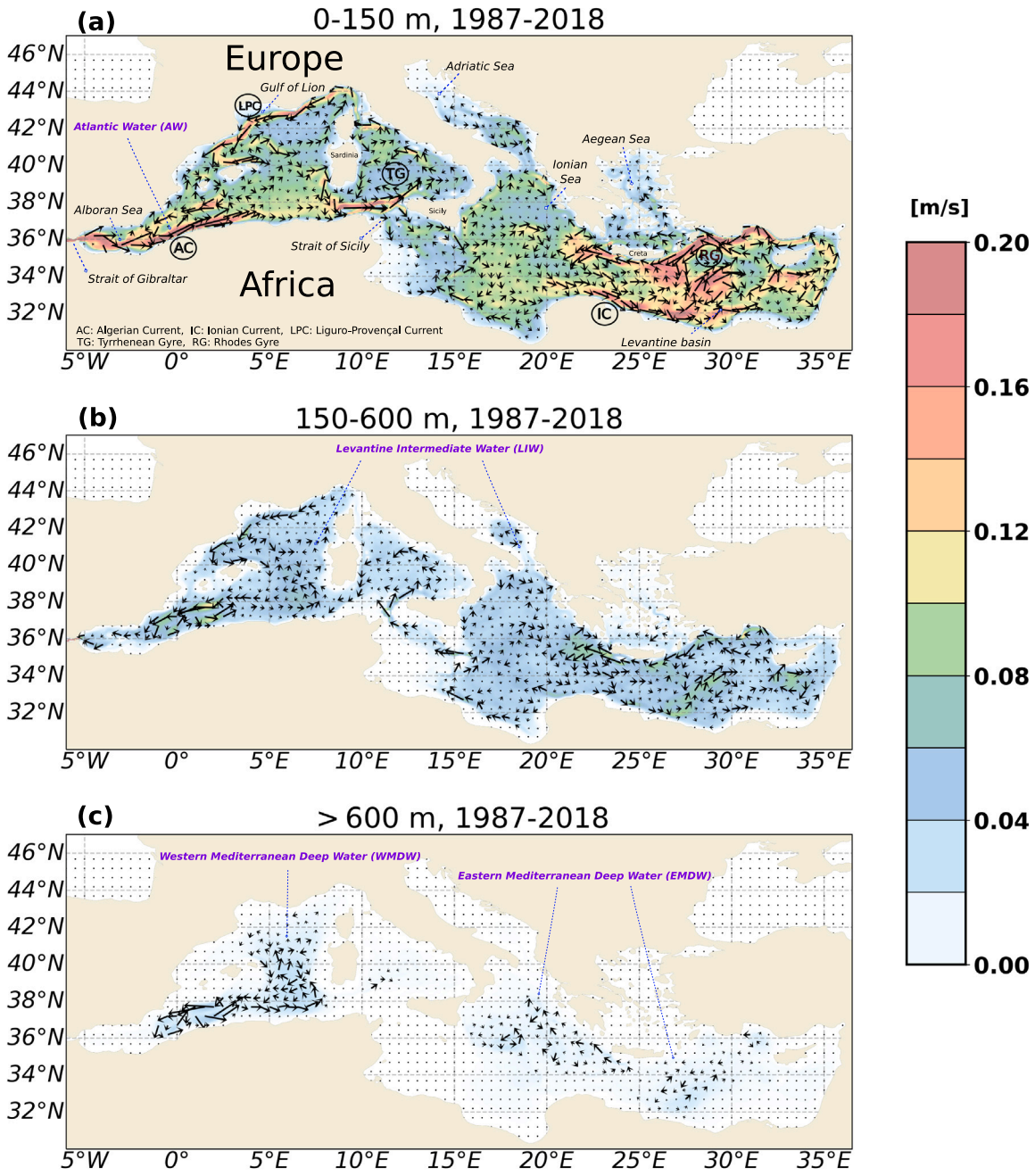

Fig. 1. Mean vertically-averaged horizontal (u, v) velocity field from years 1987 to 2018 (both included) for three depth layers: (a) 0–150 m; (b) 150–600 m; (c) > 600 m. Color denotes the current speed. The main geographical and circulation features are highlighted. Note that arrow scale is different in each panel. Unit in m s^{-1}.

equations on spherical coordinates. Monthly mean fields of horizontal ocean currents (u, v), potential temperature (θ) and salinity (S) are provided for 32 years (1987–2018) with a horizontal resolution of $\frac{1}{16°} \times \frac{1}{16°}$ for 72 vertical unevenly spaced levels down to 5000 m. The model uses vertical partial cells to represent the bottom and the Jackett and Mcdougall (1995) equation of state. The domain of the model is 6°W–36.25°E in longitude, and 30.1875°N–45.9375°N in latitude. Potential density fields, ρ, are computed from θ and S fields through the Fofonoff and Millard (1983) expression.

The oceanic reanalysis model is forced by ERA-interim atmospheric momentum, heat, and freshwater fluxes (Dee and Coauthors, 2011), while the annual rainfall cycle is derived from Xie and Arkin (1997). This simulation uses a 3D variational method to assimilate in situ vertical profiles of temperature and salinity from MBTs, XBTs, CTDs, ARGO floats, bottles, and sea level anomaly (SLA) from available satellites (Dobricic and Pinardi, 2008). In situ data mainly comes from the MEDAR/MEDATLAS dataset (Maillard and Coauthors, 2005). Satellite-based sea surface temperature is used to reduce heat flux bias at the air–sea interface. The reanalysis was initialized in January 1985 using temperature and salinity climatology obtained from in situ data collected from year 1900 to the beginning of the reanalysis. Years 1985–86 are considered as a spin up period for the system and are not used in the following analysis. Additionally, heat fluxes from ERA-interim model are used to track the evolution of winter deep convection sites in the Mediterranean Sea. The ERA-interim simulation has a global coverage with 6-hourly fields provided with a horizontal resolution of 0.75° by the European Centre for Medium-Range Weather Forecasts (ECMWF).

2.2. Climate indices

Major changes in overturning circulation in a semi-enclosed basin such as the Mediterranean Sea are expected to be, to some extent, atmospherically-forced. We explore in Section 5 how the interannual overturning variability is connected with the main modes of atmospheric variability over the Mediterranean Sea. According to the recent work of Criado-Aldeanueva and Soto-Navarro (2020) the most relevant indices affecting the Mediterranean region are: East Atlantic–Western Russia (EA–WR) pattern, the North Atlantic oscillation (NAO), East Atlantic (EA) pattern, the Mediterranean oscillation indices (MOI), and the Scandinavian (SCAND) pattern. The latter has been reported to play a minor role in atmospheric forcing over the Mediterranean Sea (Josey et al., 2011). In this work we use time series provided by the National Oceanic and Atmospheric Administration (NOAA) Climate Prediction Centre (CPC). All indices except MOI were obtained from an analysis of monthly mean 500 mb height anomaly through a rotated principal component analysis (Noaa, 2008; Barnston and Livezey, 1987). In this work we use two MOI indices (Palutikof et al., 1996; Conte et al., 1989; Palutikof, 2003): the MOI_1 defined as the normalized pressure difference between Algiers (36.4°N, 3.1°E) and Cairo (30.1°N, 31.4°E); and a variant of the index, named MOI_2, calculated from Gibraltar's northern frontier (36.1°N, 5.3°W) and Lod Airport in Israel (32.0°N, 34.5°E). Pressure data used in both versions is based on NCEP/NCAR reanalysis. MOI indices are available from the Climate Research Unit (https://crudata.uea.ac.uk/cru/data/moi/).

2.3. Computation of overturning

The overturning streamfunction (ψ) allows to quantify the strength of Mediterranean Sea thermohaline cells in both zonal and meridional directions. With this metric, zonal (meridional) eastward and westward (northward and southward) flows can be identified, as well as the depth and thickness of cells at which transport takes place (Lozier et al., 2019; Pinardi et al., 2019).

2.3.1. Depth space

The overturning streamfunction, ψ, is obtained in depth space from the running meridional (zonal) integral of the vertical integral of the zonal (meridional) velocity from the southern (western) boundary of our domain, i.e.,

$$\psi_{\mathrm{zon}}(x,z,t) = -\int_{y_B}^{y_T}\int_{-H}^{z} u(x,y,z',t)\,dz'\,dy \tag{1}$$

$$\psi_{\mathrm{mer}}(y,z,t) = -\int_{x_W}^{x_E}\int_{-H}^{z} v(x,y,z',t)\,dz'\,dx \tag{2}$$

where $u(x,y,z',t)$ and $v(x,y,z',t)$ are zonal and meridional monthly mean velocity components at each model grid cell, ψ_{zon} and ψ_{mer} refer to zonal and meridional overturning, respectively. $H(x,y)$ refers to the bottom depth, whose value is also different for each model cell. y_B and y_T refer to bottom and top latitudinal bounds, which change with longitude. x_W and x_E refer to western and eastern bounds, which change with latitude.

2.3.2. Potential temperature, salinity and potential density spaces

The overturning can also be extended to potential temperature (θ), salinity (S) and potential density (ρ) spaces. For instance, Pinardi et al. (2019) computed the residual overturning considering potential density and then mapped it to depth. Another approach to compute overturning considering thermohaline properties is the one described in Zika et al. (2012), where overturning circulation is computed in $\theta - S$ space.

In this work we use a half-way approach with respect to Zika et al. (2012), Pinardi et al. (2019), since we compute transport in hybrid coordinates: in x-axis we keep the geographical coordinates (latitude or longitude), and in y-axis we keep the thermohaline property of interest (θ, S or ρ). To this end, given the original zonal and meridional monthly mean velocity components at every cell, $u(x,y,z,t)$ and $v(x,y,z,t)$, we first weight velocities by their corresponding z-layer thickness, obtaining as a result a flux (unit in $m^2\ s^{-1}$). After that, velocities in z coordinate (depth) are converted to zonal ($\mathcal{U}$) and meridional ($\mathcal{V}$) fluxes in θ, S or ρ coordinates. Next, we integrate the flux over a series of selected intervals of ρ, θ, and S. Limits of those intervals are chosen considering all time minimum and maximum values of ρ, θ, and S. To compute the transport, we use intervals of 0.1 for potential density and potential temperature, and 0.05 for salinity.

Potential temperature

$$\text{Zonal}: \quad \psi_{\mathrm{zon},\theta}(x,\theta,t) = -\int_{y_B}^{y_T}\int_{\theta_{max}}^{\theta} \mathcal{U}(x,y,\theta',t)\,d\theta'\,dy \tag{3}$$

$$\text{Meridional}: \quad \psi_{\mathrm{mer},\theta}(y,\theta,t) = -\int_{x_W}^{x_E}\int_{\theta_{max}}^{\theta} \mathcal{V}(x,y,\theta',t)\,d\theta'\,dx \tag{4}$$

Salinity

$$\text{Zonal}: \quad \psi_{\mathrm{zon},S}(x,S,t) = -\int_{y_B}^{y_T}\int_{S_{min}}^{S} \mathcal{U}(x,y,S',t)\,dS'\,dy \tag{5}$$

$$\text{Meridional}: \quad \psi_{\mathrm{mer},S}(y,S,t) = -\int_{x_W}^{x_E}\int_{S_{min}}^{S} \mathcal{V}(x,y,S',t)\,dS'\,dx \tag{6}$$

Potential density

$$\text{Zonal}: \quad \psi_{\mathrm{zon},\rho}(x,\rho,t) = -\int_{y_B}^{y_T}\int_{\rho_{min}}^{\rho} \mathcal{U}(x,y,\rho',t)\,d\rho'\,dy \tag{7}$$

$$\text{Meridional}: \quad \psi_{\mathrm{mer},\rho}(y,\rho,t) = -\int_{x_W}^{x_E}\int_{\rho_{min}}^{\rho} \mathcal{V}(x,y,\rho',t)\,d\rho'\,dx \tag{8}$$

where θ_{max}, S_{min}, and ρ_{min} refer to maximum potential temperature, minimum salinity and minimum potential density. We note that the running integral could also start from the bottom upwards, and could be computed using the vertical velocity (Lozier et al., 2019; Sayol et al., 2019).

3. Mean Mediterranean Sea circulation and overturning streamfunction

In this section we first show the mean Mediterranean Sea circulation provided by model data. Then zonal and meridional mean overturning circulation patterns are shown for depth, potential density, potential temperature and salinity spaces.

3.1. Mean circulation

The mean vertically integrated horizontal velocity field provided by the reanalysis is shown in Fig. 1 for different depths: (a) 0–150 m, (b) 150–600 m, and (c) 600 m to the bottom depth. In the upper range, the eastward AW moves towards the Strait of Sicily as the Algerian Current (AC). An AC branch is deflected towards the interior before reaching the Sardinia Channel, while another branch contributes to form the Tyrrhenian Gyre (TG). In the Strait of Sicily the AC is divided into boundary and interior paths that eventually converge downstream to form the Ionian Current (IC) in the Ionian Sea. After reaching the eastern boundary in the Levantine Basin, the IC returns back westward along the northern boundary, finding on its way the cyclonic Rhodes Gyre (RG). Some of those waters sink and join deeper water masses originated during winter convection to form the LIW (Fig. 1b). After crossing the Ionian Sea, part of the AW and LIW surrounds the Adriatic Sea to finally reach back the western sub-basin. There the AW evolves in the Liguro-Provençal Current (LPC, also called Northern Current), which sinks on its way along the northwestern sub-basin off French and Spanish coasts. Eventually, a substantial volume of water mass

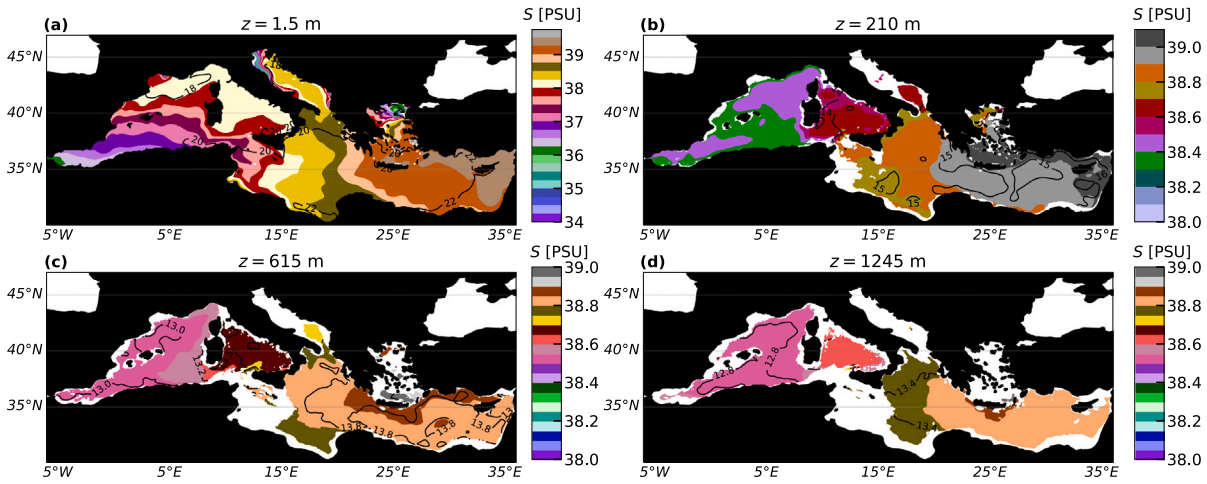

Fig. 2. Maps showing the mean salinity (color) and potential temperature (black contours) between years 1987 and 2018 (both included) for several depths: (a) 1.5 m, (b) 210 m, (c) 615 m and (d) 1245 m.

escapes through the Strait of Gibraltar (Fig. 1b). Distinctly, in the bottom layers the circulation is depicted by three cyclonic cells that carry out deep colder waters (Fig. 1c), one larger in the middle of the western basin, and two other in the eastern basin: one in the Ionian Sea, and another one around the Rhodes Gyre (RG). For a further description of Mediterranean Sea circulation features we refer the reader to Millot and Taupier-Letage (2005), Millot and Gerin (2010) and Bergamasco and Malanotte-Rizzoli (2010).

Regarding water mass properties, there are large mean meridional and zonal differences of potential temperature and salinity in the upper layers (Fig. 2a–b) that can reach up to $\Delta S = 4$ and $\Delta\theta = 4\,^{\circ}\mathrm{C}$ at the surface respectively, with maximum mean potential densities over $1027.5\,\mathrm{kg\ m^{-3}}$ (not shown). Zonal differences also exist at deep layers, with mean values of about $\Delta S = 0.2$ and $\Delta\theta = 0.8\,^{\circ}\mathrm{C}$ (and maximum mean potential densities of $1029.3\,\mathrm{kg\ m^{-3}}$) at $z = 1245$ m (Fig. 2c–d). Water mass properties take values within the range of variability previously reported in the literature (Schroeder et al., 2016; Mauri et al., 2019; Menna et al., 2021), thus depicting the classical picture in which AW tends to get colder and more saline as it recirculates along the Mediterranean Sea favored by the larger winter heat loss and the higher rates of summer evaporation, especially in the Eastern Mediterranean.

3.2. Mean overturning circulation

Depth space

Mean zonal and meridional overturning stream functions in depth space for years 1987–2018 are shown in Fig. 3a-b, respectively. Note that positive (negative) values are associated with clockwise (counterclockwise) water mass displacements. Fig. 3a draws the traditional clockwise basin-scale cell in the upper layers (reddish) depicting the AW moving eastward and then returning deeper (0–200 m). At larger depths there are three cells, one counterclockwise in the Western Mediterranean, across the Algerian Basin and the Gulf of Lions, that extends to the Tyrrhenian Sea with a transport of −0.7 Sv (i.e., the maximum of the counterclockwise circulation) near 1500 m depth; and two in the Eastern Mediterranean sub-basin: one strong clockwise cell between the Adriatic and the Aegean Sea with maximum transport of 1.2 Sv at 1000–2000 m depth, and another much weaker counterclockwise one of ∼ −0.15 Sv in the Levantine basin (we highlight that deeper cells are associated with the mean circulation shown in Fig. 1c), constrained by bathymetric features. In contrast, the meridional overturning depicts a more complex pattern (Fig. 3b). First, there is a near-surface (0–200 m depth) counterclockwise cell that extends from the south to the center of the basin (upper bluish shape). This structure is followed by a deeper clockwise cell that reaches 1000 m depth in some locations, with its maximum value occurring around 36°N at subsurface layers (reddish). Finally, a large counterclockwise cell fills the center of the basin below 500 m depth, reaching its largest transport at 1500–2000 m depth (−1.1 Sv). For the sake of comparison, a map of vertical velocities at about 1000 m depth derived from the continuity equation for this ocean reanalysis, as in Fig. 6 of Pinardi et al. (2019), is shown in Fig. S1.

The above meridional picture, which to our knowledge was first shown by Pinardi et al. (2019), and then by Lyubartsev et al. (2020), is now zoomed at sub-basin scale in Fig. 4a-b for both Western Mediterranean (WMED) and Eastern Mediterranean (EMED) seas, respectively. In the WMED case, the northward (positive) near-surface Algerian Current appears clearly depicted at a latitude between 36–38°N, while the negative patch at latitudes over 38°N represents the Liguro-Provençal Current. At higher latitudes, the subsurface current shows a positive kernel near 500 m depth that extends up to 2 km depth. Thus, this clockwise cell includes the northward Levantine Intermediate Water (LIW) moving northwestward from Italian to French coasts and, at deeper layers, the Western Mediterranean Deep Water (WMDW). The counterclockwise cell that appears at deeper layers is more related with diabatic mixing and cross-isopycnal transport driven by topographic features (Pinardi et al., 2019). This cell is specially strong in the half-lower side (36–38°N). In the EMED the signature of the Ionian Current moving southeastward appears between 31–38°N, while between 200–800 m depth shows up the signature of the LIW moving northwestward and recently formed deep waters in the Adriatic Sea. Finally, there appears a strong deeper circulation characterized by a counterclockwise cell in the northern part of EMED associated with intermediate and deep water formation in the Aegean Sea (EMDW, bluish patch in Fig. 4b, also depicted in Fig. 1c) in which the transport is southward at intermediate depths and northward near the bottom.

Potential density (ρ) space

Mean zonal and meridional overturning in density space are shown in Fig. 3c–d, respectively. The complex zonal circulation seen in depth space is now reduced to one big clockwise cell that extends from the Alboran Sea to the Levantine Basin with a maximum mean transport of ∼ 1.1 Sv. Overall water mass gets denser on its way towards the EMED (up to $3\,\mathrm{kg\ m^{-3}}$), reaching the highest densities in the surroundings of the Cretan Passage with values that on average can surpass $1029\,\mathrm{kg\ m^{-3}}$. Interestingly, densities tend to maintain for water masses that move westward from the Ionian Sea, which suggests a dominant isopycnal displacement. A very weak counterclockwise transport also emerges in

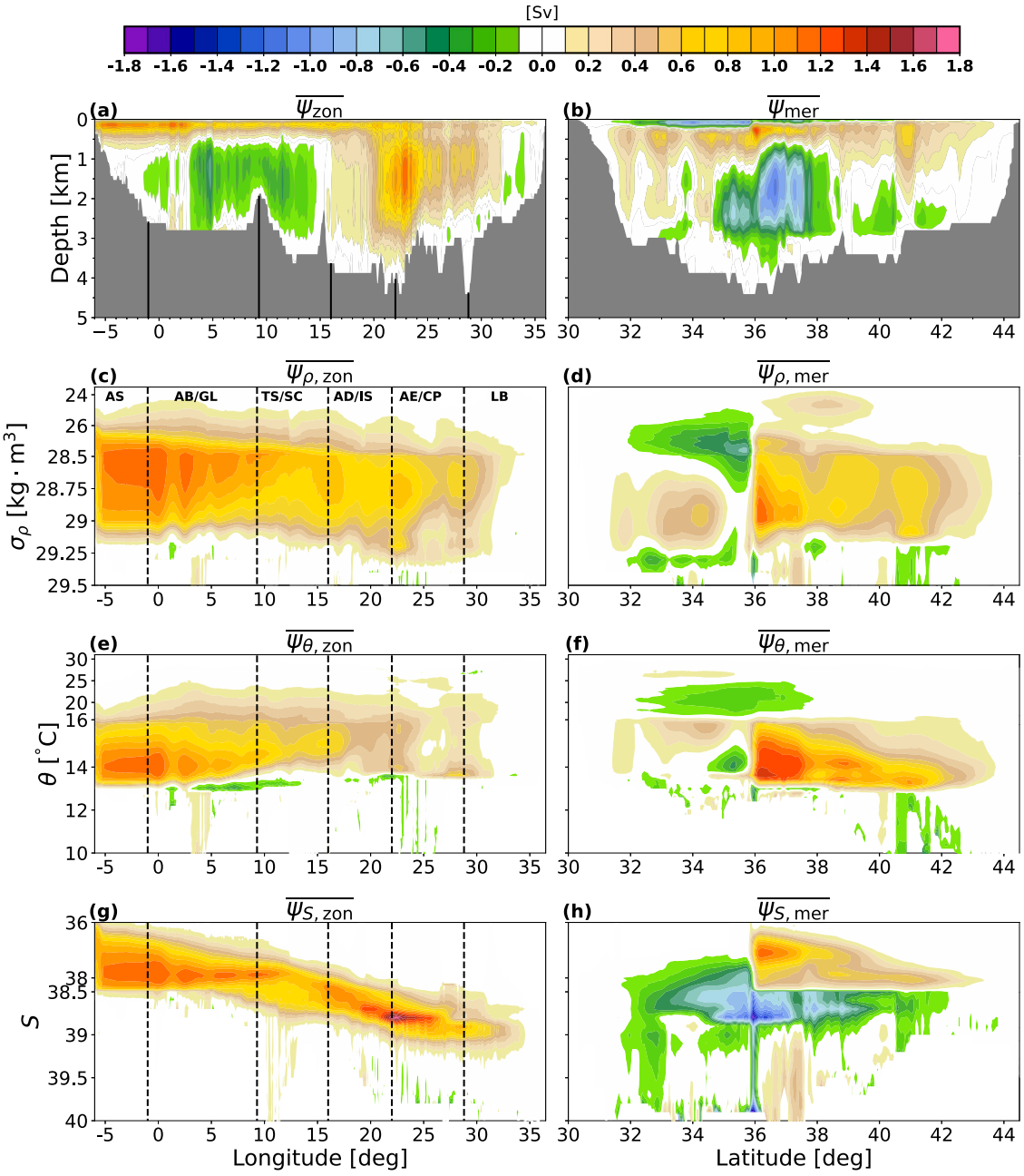

Fig. 3. Mean Mediterranean Sea overturning circulation between years 1987 and 2018 (both included) computed from model data following Eqs. (1)–(8). Zonal (left panels), and meridional (right panels) overturning transports are shown for: depth space (first row), potential density space (second row), potential temperature space (third row), and salinity space (last row). Regional sub-basins are depicted as inset panels in figures of meridional overturning. Unit in Sv. Note that yellowish-reddish (greenish-bluish) color means clockwise (counterclockwise) stream currents. Regarding the clockwise cell, when transport increases (decreases) along y-axis it means that an eastward (westward) current is present. The opposite occurs for a counterclockwise cell. When color does not change along y-axis it means that no extra transport is being added to overturning. Acronyms: AS = Alboran Sea, AB = Algerian Basin, GL = Gulf of Lion, TS = Tyrrhenian Sea, SC = Strait of Sicily, AD = Adriatic Sea, IS = Ionian Sea, AE = Aegean Sea, CP = Creta Passage, LB = Levantine Basin.

the bottom layers of the WMED and EMED linked to the densest water masses ($\rho > 1029.2\,\mathrm{kg\ m^{-3}}$ (depicted by small green patches in Fig. 4c).

In the meridional direction the circulation is much more complex as there are different cells at each sub-basin (Fig. 4c-d). In the WMED there are two main clockwise cells (waters get denser as they move northward): one intense between 36–37.5°N (kernel transport larger than 1.2 Sv) associated with AW, and another one weaker between 38–44°N (kernel transport smaller than 0.8 Sv) with two kernels: one at about 1028.75 kg m^{-3} representing the LIW, and another one for a density close to 1029.1 kg m^{-3} associated with the WMDW. Similarly to depth space, there also appears a weaker counterclockwise cell that contains denser waters. In the Eastern Mediterranean there are at least four main different cells: one large counterclockwise cell between 32–38°N with minimum values of −0.9 Sv (waters get up to 3 kg m^{-3} denser as they move southward) associated with the Ionian Current; two deeper clockwise cells (located at 32–35°N and 37.5–39°N, respectively) connected with LIW and denser waters with a mean maximum transport close to 0.6 Sv and smaller associated density

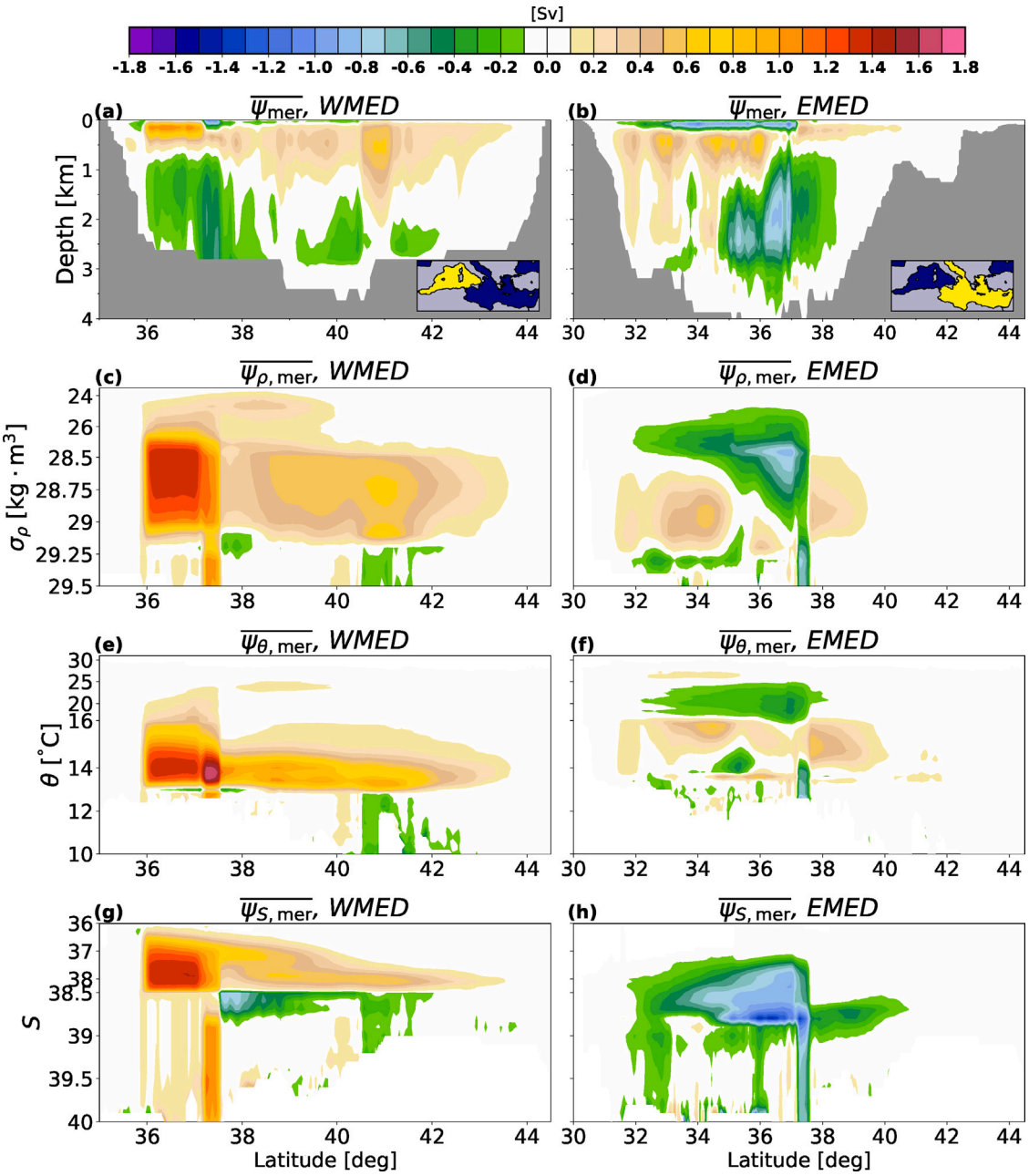

Fig. 4. Meridional overturning circulation between years 1987 and 2018 (both included) distinguishing for Western Mediterranean (WMED, left panels) and Eastern Mediterranean (EMED, right panels) sub-basins. Meridional transports are shown for: depth space (first row), potential density space (second row), potential temperature space (third row), and salinity space (last row). Note that reddish (bluish) color means clockwise (counterclockwise) transport. Areas used for the computation of overturning in each sub-basin are yellowish in the inset panels included in the first row.

changes (0.5 kg m^{-3}); and the deepest cells associated to EMDW, with densities of around 1029.2 kg m^{-3} and above.

Potential temperature (θ) space

The zonal mean overturning in potential temperature space is characterized by a clockwise cell that extends from the Alboran Sea to the Levantine Basin (Fig. 3e). The maximum mean transport is about 1.2 Sv, being located in the WMED, with the main kernel at θ = 14–15 °C. Mean zonal overturning transport in the EMED is 2–3 times weaker, showing a less coherent spatial pattern. Overall, Atlantic waters entering through the Strait of Gibraltar tend to get warmer on their way across the Alboran Sea, and then their temperature tends to decrease at a slower rate as they move towards the EMED. Hence, the largest amount of water cooling seems to occur, on average, in the WMED (Fig. 3e). Additionally, there is a remarkable counterclockwise cell in the WMED containing a bulk of homogeneous cold waters (green tongue-like shape, likely formed by residual WMDW) with a temperature of around θ = 13 °C. A counterclockwise, weaker cell, formed by slightly warmer waters is revealed again in the EMED.

As in the potential density case, the meridional overturning is rather more complex as it is formed by different cells, depending on the latitude and on the water mass properties (Fig. 3f). Indeed the number and distribution of cells follow a similar pattern to that seen in potential density space. In the WMED there is a clear dominant clockwise cell reaching transport values over 1.3 Sv at a latitude of 37.5°N (Fig. 4e), while in the EMED there are at least three main cells: one larger counterclockwise cell formed by lighter waters with a minimum mean of −0.6 Sv (θ = 17–26 °C), a clockwise cell with two kernels (one close

to 34°N, and another one close to 38°N) formed by colder waters (θ = 15–17 °C) with a maximum mean magnitude of overturning transport of about 0.4 Sv (Fig. 4f), and finally more localized counterclockwise cells with the coldest waters (θ < 15 °C).

Salinity (S) space

Again, the mean zonal overturning pattern in S space is similar to that of potential density (compare Fig. 3g with Fig. 3c), which is characterized by a well-defined clockwise transport cell of water mass that gets substantially more saline as it recirculates through the Mediterranean Sea (from around S = 36 to 39), with its largest transport (maximum over 1.5 Sv) located between the Adriatic Sea and the Cretan Passages (21–25°E), within the regions of intermediate and deep water formation. Regarding the meridional overturning pattern, it is also more complex than the zonal one in salinity space (Fig. 3h), with a distinguishing behavior at sub-basin scale characterized by strong clockwise (one big for S < 38.5 and another smaller one for S > 38.5, with a transport close to 1 Sv) and counterclockwise cells in the WMED between 37–42°N (Fig. 4g); and by a notable counterclockwise cell in the EMED between 32–40°N (Fig. 4h), with largest values close to −1 Sv, respectively.

4. Seasonal variability of Mediterranean Sea overturning

In this section we first provide time series of maximum and minimum monthly Mediterranean Sea overturning for all spaces. Seasonal variations are also explored in terms of spatial patterns.

4.1. Monthly time series

Monthly time series of maximum (associated to clockwise cells) and minimum (associated to counterclockwise cells) zonal and meridional overturning are shown in Fig. 5 (red and blue lines, respectively) for WMED and EMED sub-basins (left and right panels, respectively) and for all spaces (note that peaks may belong to different grid cells every month). Time series are shown for all spaces: depth (a–b), potential density (c–d), potential temperature (e–f) and salinity (g–h). Overall time series are rather noisy with mean values within ±1.5 Sv. The range of variability spans from −5 to 5 Sv in depth space and from −10 to 10 Sv in the rest of spaces. The largest magnitude (in absolute value) is found in density space for the WMED and in salinity space for the EMED, respectively. Note that an episode of strong overturning in one given space is not necessarily accompanied by simultaneous large variations in other spaces (e.g., see the strong peak in salinity space in 2001–2002 in the WMED). From Fig. 5 it is clear that the variance is larger in the EMED, especially in salinity space. Among the strongest events to mention, it is possible to identify the Eastern Mediterranean Transient (EMT) in the EMED between 1993 and 1996 with peaks in all spaces although at different times for zonal and meridional components, being the peak in the meridional overturning earlier (from a few months up to 2 yr sooner). In the WMED is easy to recognize the 2004–2006, 2012–2013 and 2017–2018 convection events. These results evidence the sensitivity of overturning metric to capture transport variations associated to monthly water mass changes. In Section 5 a detailed analysis of the 2004–2006 WMED event is provided, since it represents the start of the Western Mediterranean Transition (WMT).

4.2. Seasonal variability

Annual peaks of maximum and minimum transport associated with the annual cycle emerge in Fig. 5. To better explore these variations we have depicted the climatological seasonal mean for years 1987–2018 of zonal (Fig. 6) and meridional (Figs. 7–8) overturning for all spaces. As seen, zonal overturning transport is stronger in the upper layers during winter months in depth space (Fig. 6a), to later decrease during summer (Fig. 6c). In intermediate and deep layers the largest magnitude of zonal overturning in depth space occurs during autumn and winter months for the WMED and EMED, respectively. In density space a strong transport (> 1.2 Sv) is found during winter months between 2–12°E (in the central WMED) and between 22–28°E (in Ionian and Aegean seas and in the Cretan Passage), close to areas of strong convection. The magnitude of overturning decreases during the rest of the year, reaching its minimum during summer in all spaces. This decrease is more remarkable in the EMED, where maxima are around half of the magnitude of winter maxima in potential density space. These results suggest the preeminent role of winter atmospheric cooling in exacerbating the formation of large volumes of dense waters ($\rho \approx$ 1028.5–1028.9 kg m^{-3}). A similar behavior is found in potential temperature and salinity. It is remarkable the stability of the spatial distribution of salinity overturning cell since it keeps its area all the year round (Fig. 6m–p), while the extension of the area with relevant transport changes notably for potential density (Fig. 6e–h) and potential temperature (Fig. 6i–l) spaces between winter and summer months.

As in the zonal overturning, the largest transport in the meridional component also tends to occur during winter in both sub-basins (Fig. 7 and 8, respectively). Regarding the WMED we note the presence in all spaces of a strong quasi permanent surface cell at lower latitudes between 36–37.5°N, likely associated with the Algerian Current (Fig. 7). Another cell at higher latitudes exists (around 40.5–41.5°N, associated with LIW and WMDW) with a strong seasonal cycle. The magnitude of the latter appears to be weaker in both depth and salinity spaces (< 0.7 Sv) than in potential density (1.2 Sv) and potential temperature spaces (2.2 Sv in winter, Fig. 7e,i). The large volume of cold waters depicted in potential temperature space tends to generally be clockwise (warmer water masses move southward whereas deeper water masses move northward). It weakens to about 0.8 Sv during summer months in the northern WMED. The picture is different in EMED since a strong transport in potential temperature space centered at $\theta \approx$ 16 °C and 34.5°N is accompanied by a large transport in salinity space (with positive and negative sign, respectively) driven by water mass with $S \approx$ 38.9 (although the range of variability spans from S = 37 up to S = 39.2). A clockwise cell with maxima close to 0.8 Sv (located around 34.5°N) in potential density space is associated to LIW, with $\rho \approx$ 1029 kg m^{-3}. As for the zonal overturning, the cell expands during summer for potential density and potential temperature due to the existence of lighter (warmer) waters in the upper layers. Interestingly, during winter water masses become more homogeneous, especially in potential temperature space, disappearing the upper counterclockwise cell (Fig. 8i).

From another perspective, Fig. 9 shows the mean (black lines) and the 32-year climatology (*i.e.*, mean of all Januaries, all Februaries, etc, depicted by gray lines) overturning vertical profiles depicted for selected locations where a large transport is found (depicted by magenta dashed lines in Figs. 6–8). Zonal (first two columns) and meridional (last two columns) illustrate the range of variability, being these months of maximum and minimum transport (in absolute value) indicated in each panel. As expected, an eastward transport in the upper layers (first 200 m in the WMED) is compensated by a westward transport in deeper layers (Fig. 9a-b) with seasonal variations of around 0.3 Sv. In potential density space seasonal changes are larger, surpassing 1 Sv in some locations (Fig. 9e–h). A similar range of variability around the maxima is found for potential temperature and salinity spaces (Fig. 9). Note the seasonal change in the sign of potential temperature in the EMED (Fig. 9i).

5. Interannual variability of overturning

In this section we explore the interannual variability of Mediterranean Sea circulation from an overturning circulation perspective. First, we provide the range of variability of overturning in all spaces from zonal and meridional directions. Next, we study the quasi instantaneous connection between the inter-annual signals of transport (in

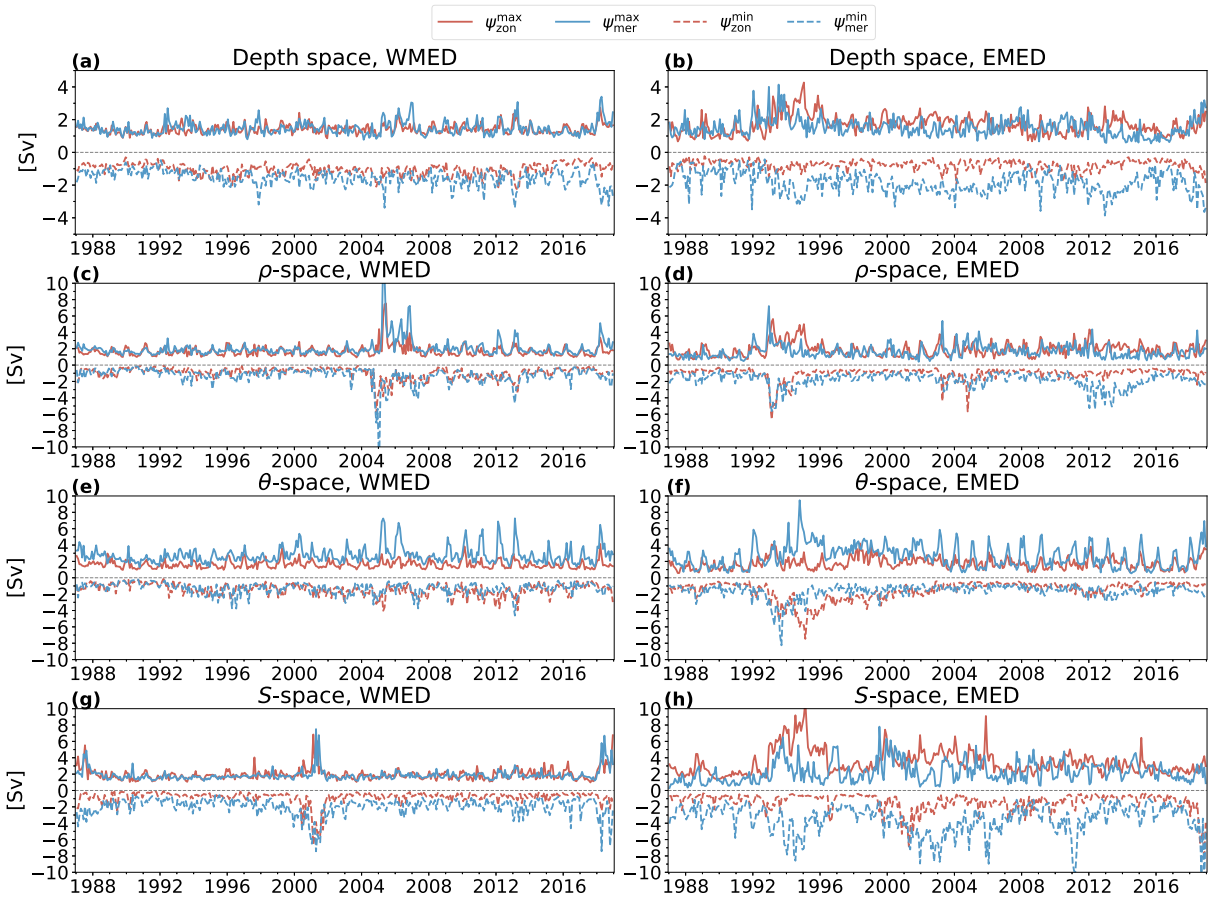

Fig. 5. Time series of maximum (solid line) and minimum (dashed line) monthly overturning for zonal (red) and meridional (blue) overturning considering: (a) the WMED, and (b) the EMED. Time series cover the period 1987–2018 (both included).

both depth and density spaces) and the main climate indices that influence Mediterranean Sea atmospheric dynamics. Finally, we analyze in detail how the strong deep convection event that took place in winters of years 2005 and 2006 is depicted in terms of overturning.

As the maps of interannual variability of overturning in depth space were already presented by Pinardi et al. (2019), we here focus on those of potential density, potential temperature and salinity. The yearly zonal mean overturning transport in density space is shown in Fig. 10. The overturning has the shape of a zonal cell where water masses densify as they move towards the east. As seen, transport varies from year to year, ranging between a weaker and smaller cell (year 2015), and a stronger and larger cell that extends close to the eastern boundary (year 1996). The maximum value is reached in the EMED during years 1993 and 1994, where values over 2.5 Sv are obtained. Maxima are located in the Aegean Sea and Cretan Passages in 1993, then they spread towards the west till reaching the Adriatic and Ionian Seas in 1994 (Fig. 10, bottom panel). This extraordinary densification ($\sigma_\rho \sim 29\,\mathrm{kg\ m^{-3}}$) is in good agreement with the EMT, and it does not occur again in the model simulation, where the annual maximum zonal overturning has remained below 2 Sv. These patterns are also reflected in potential temperature and salinity space, where a large volume of cold and salty waters ($\theta \approx 14\,^\circ\mathrm{C}$ and $S \approx 38.5$) form in the Aegean Sea and Cretan Passage between years 1992 and 1995 (maximum value > 3.5 Sv), to later move to the Ionian and Adriatic seas (Fig. S2-S3). As mentioned above, the meridional component detects one year earlier the EMT. In particular, it is depicted by an anomalous clockwise cell of dense waters ($\sigma_\rho \sim 29\,\mathrm{kg\ m^{-3}}$, reddish shading) that dramatically strengthens during years 1992 and 1993 at 34–36°N, which mainly corresponds to the Cretan Passage, and the southern Aegean Sea (Fig. S4). This clockwise cell is accompanied by a stronger counterclockwise cell that covers the Aegean Sea and the Levantine Basin. In terms of potential temperature it is even clearer, since a large clockwise strong cell (maximum close to 2 Sv) suddenly forms in 1992, between 32–36°N (Fig. S5). In contrast, differences in terms of salinity are less obvious (Fig. S6).

Regarding the WMED, the annual mean meridional overturning shows a relatively large clockwise cell (lighter waters move northward and denser waters southward) in the southern part of the basin with a mean annual maximum ranging between 1.2 and 1.8 Sv (Fig. S7). In the northern part, the imprint of intense deep water convection events are clearly distinguishable in density space for years 2005–2006, 2012–2013 and 2018 (note the reddish shading around 41°N), where the transport of dense waters intensifies ($\sigma_\rho \sim 28.9\,\mathrm{kg\ m^{-3}}$). In terms of potential temperature and salinity, a strengthening of the northern cold clockwise cell (between 38.5–41°N) is found during years 2005, 2006 and 2012 for water masses of around $\theta = 14\,^\circ\mathrm{C}$ and $S = 38$–38.5 with values over 2 Sv (Fig. S8 and S9). A more detailed analysis of the winter deep convection event of winters of years 2005 and 2006 is presented later.

5.1. Quasi-instantaneous influence of interannual climate signals on overturning transport

Because the extraordinary convection events caused by atmospheric cooling take place during winter, we will restrict our study to investigate the "quasi-instantaneous" influence of climate signals on overturning during winter months (December to March). Besides, as meridional

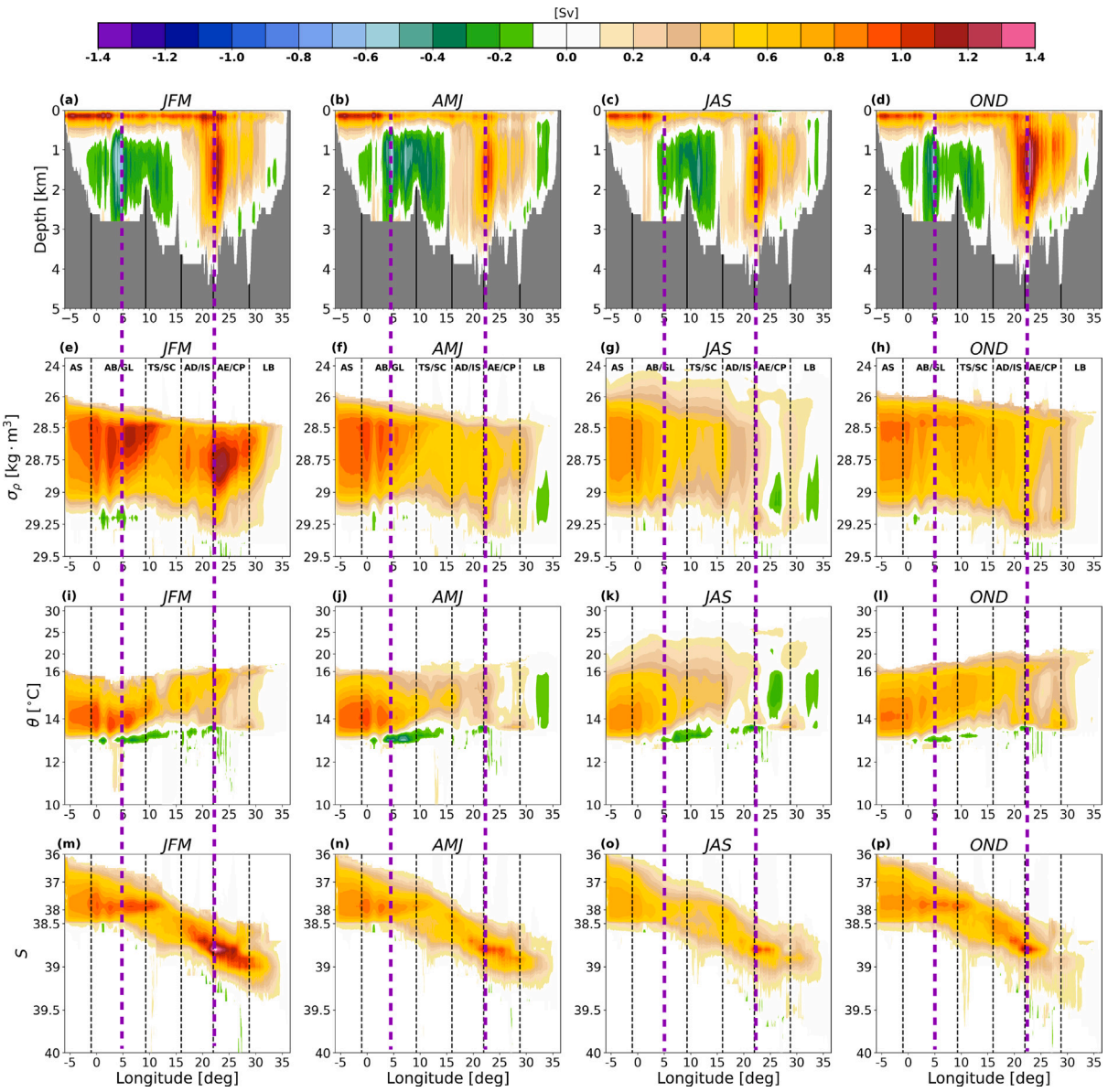

Fig. 6. Climatology of zonal Mediterranean Sea overturning between years 1987 and 2018 (both included) computed with model data. Overturning is depicted for all spaces: depth (a–d), potential density anomalies (σ_ρ) space (e–h), θ space (i–l) and S space (m–p). Unit in Sv. Note that yellowish/reddish (greenish/bluish) color means clockwise (counterclockwise) transport. Acronyms were defined in Fig. 3.

overturning responds faster to changes in water mass transport induced by intermediate and deep convection processes, we have computed the winter average of meridional overturning in depth and density space following the approach of Lyubartsev et al. (2020). Thus, we have constrained overturning transport to those regions we expect to be more affected by intermediate and deep water formation in WMED and EMED: the Gulf of Lion and the Southern Aegean Sea. In the WMED the Western Mediterranean Oscillation Index (WMOI) is computed by taking into account the maximum transport below 300 m depth at a latitude over 40°N, i.e.:

$$\mathrm{WMOI} = max\left\{\psi_{mer,W}(\mathrm{lat} \geq 40^{\circ}\mathrm{N},\ \mathrm{depth} > 300\,\mathrm{m})\right\},$$

which corresponds to the maximum value of the clockwise cell shown in Fig. 11a, in the northern part of the WMED basin, with its kernel located at about 500 m depth.

Regarding the EMED basin, the cell more sensitive to intermediate and deep water formation events is the clockwise one shown in Fig. 11b, with its maximum also located at about 500 m. In order to identify this cell we have computed the Eastern Mediterranean Oscillation Index (EMOI), defined as Lyubartsev et al. (2020):

$$\mathrm{EMOI} = max\left\{\psi_{mer,E}(\mathrm{lat} < 36.5^{\circ}\mathrm{N},\ \mathrm{all\ depths})\right\},$$

Analogously, we have defined two indices to characterize overturning variations in density space: the WMOI$^\rho$, and the EMOI$^\rho$. These indices are defined as:

$$\mathrm{WMOI}^\rho = max\left\{\psi_{\rho,mer,W}(\mathrm{lat} \geq 40^{\circ}\mathrm{N},\ \rho > 1028.5\,\mathrm{kg\ m^{-3}})\right\},$$

$$\mathrm{EMOI}^\rho = max\left\{\psi_{\rho,mer,E}(\mathrm{lat} < 36^{\circ}\mathrm{N},\ \rho > 1028.5\,\mathrm{kg\ m^{-3}})\right\},$$

and correspond to the northern clockwise cell shown in Fig. 11c and the southern clockwise cell shown in Fig. 11d, respectively. Time series of all indices are displayed Fig. 11e–f. As seen, the maximum overturning

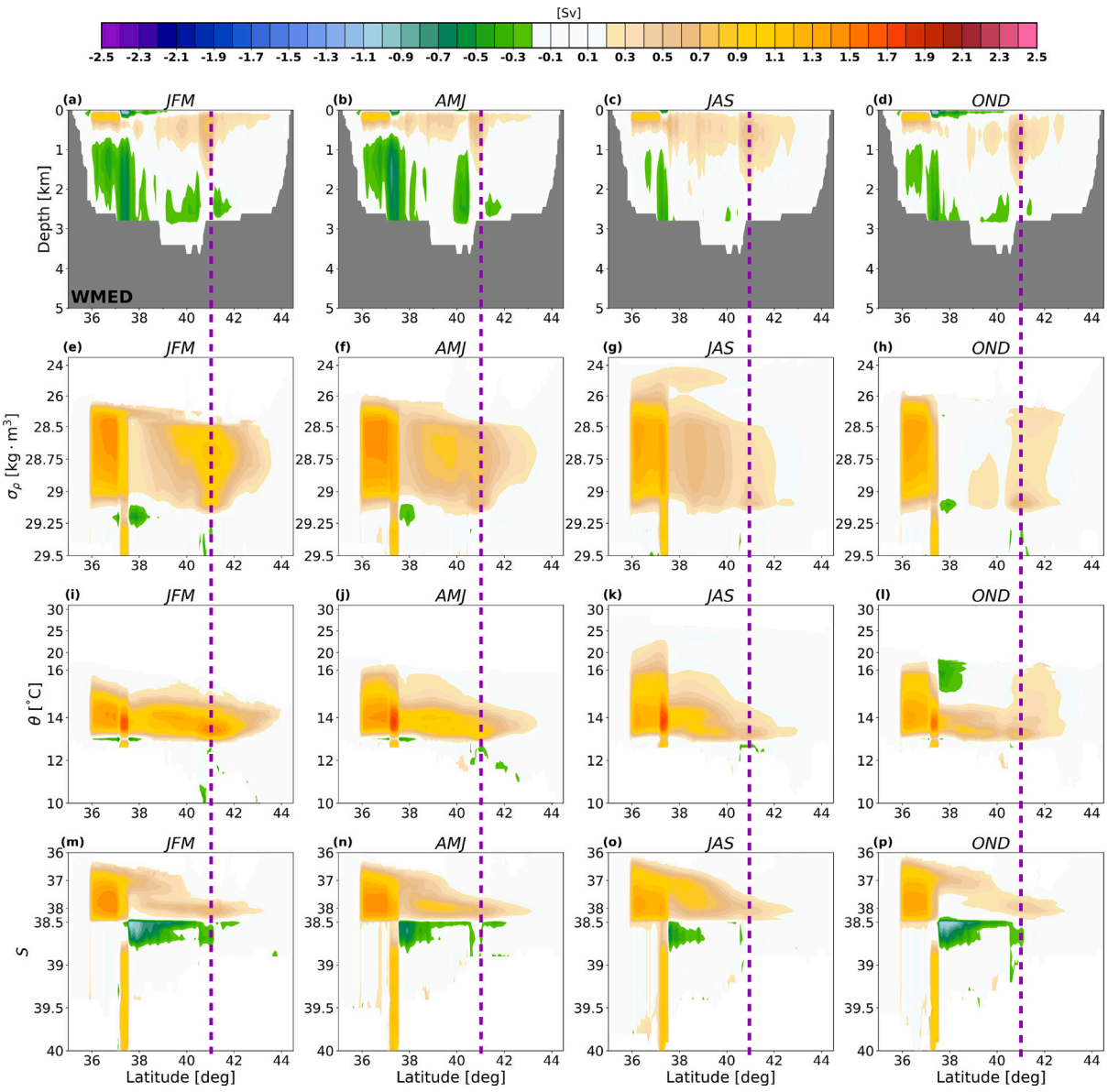

Fig. 7. Climatology of meridional Western Mediterranean (WMED) Sea overturning between years 1987 and 2018 (both included) in potential density space computed with model data. data. Overturning is depicted for all spaces: depth (a-d), potential density anomalies (σ_ρ) space (e–h), θ space (i–l) and S space (m–p). Unit in Sv. Note that yellowish/reddish (greenish/bluish) color means clockwise (counterclockwise) transport.

transport in density space is generally about 0.5–1 Sv larger than in depth space.

Next, we have correlated the above indices against the main climate signals in the region (we refer to Section 3 for further information): Eastern Atlantic Pattern (EA), Mediterranean Oscillation Index type 1 (MOI_1), Mediterranean Oscillation Index type 2 (MOI_2), the North Atlantic Oscillation (NAO), the Scandinavian (SCAND) and the East Atlantic–Western Russia pattern (EA-WR). To make indices comparable with overturning transport, annual winter averages are also computed over time series of climate indices (displayed in Fig. S10). The p-value of linear correlations is computed from a Student's t-test where the null hypothesis states that distributions underlying the samples are uncorrelated and normally distributed.

Results indicate that regarding instantaneous correlations in depth space (Table 1, WMOI and EMOI), they are only statistically significant at 95% (or 99%) for two cases: WMOI is significantly correlated with the NAO ($r = -0.36$), and EMOI is significantly correlated with EA ($r = -0.39$). In contrast, in density space (Table 1, $WMOI^\rho$ and $EMOI^\rho$) the $WMOI^\rho$ is significantly correlated with EA ($r = -0.39$), MOI_1 ($r = -0.49$), NAO ($r = -0.41$), and SCAND ($r = 0.51$); and $EMOI^\rho$ is significantly correlated with EA ($r = -0.46$) and EA-WR ($r = 0.44$). Results indicate that overturning in density space is generally better correlated with climate indices than overturning in depth space, being thus more sensitive to changes in the low atmospheric conditions over the Mediterranean Sea. In Section 6 we discuss the implications of these correlations in terms of circulation patterns.

5.2. Characterization of winter deep convection events of 2005 and 2006 in the Western Mediterranean

Unlike the EMT that took place in the 1990's (Pinardi et al., 2019; Lyubartsev et al., 2020), winter deep convection events have been poorly studied in the WMED from an overturning perspective. In this section we analyze in more detail the characteristics of the strong

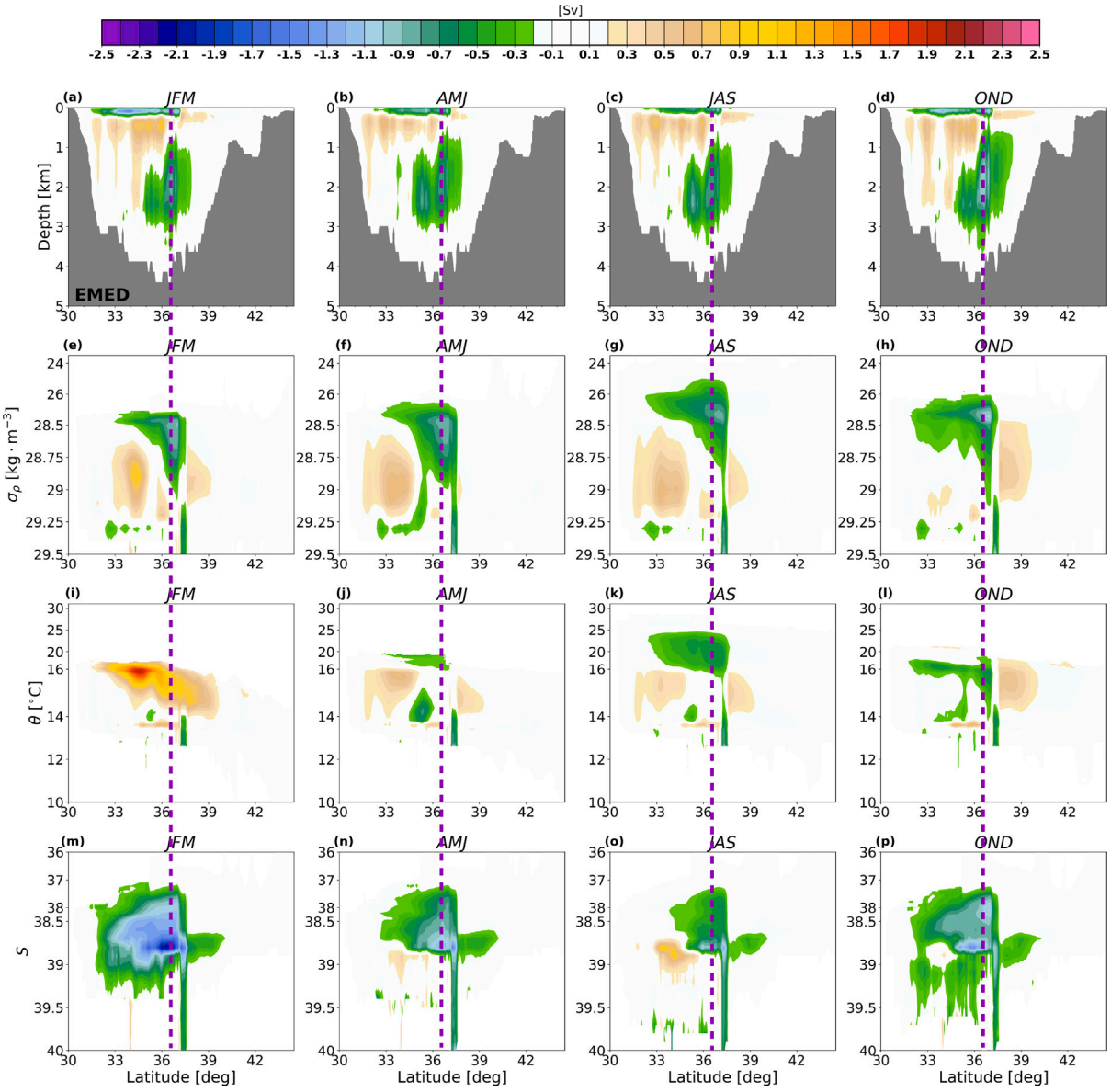

Fig. 8. Same as in Fig. 7 but for the Eastern Mediterranean (EMED) sub-basin.

Table 1
Correlations of WMOI, EMOI, WMOI$^\rho$, and EMOI$^\rho$ against selected climate indices: EA, MOI_1, MOI_2, NAO, SCAND and the EA-WR.

Component	EA	MOI_1	MOI_2	NAO	SCAND	EA-WR
WMOI	−0.23	−0.33	−0.16	−0.36*	0.34	0.01
EMOI	−0.39*	0.24	−0.01	−0.09	0.03	0.28
WMOI$^\rho$	−0.39*	−0.49**	−0.26	−0.41*	0.51**	−0.13
EMOI$^\rho$	−0.46**	−0.27	0.05	−0.06	−0.06	0.44*

*Pearson correlation is statistically significant at 95% according to a Student's t test.
**Pearson correlation is statistically significant at 99% according to a Student's t test.

events that took place in the surroundings of the Gulf of Lion in winter of years 2005 (December 2004 to March 2005) and 2006 (December 2005 to March 2006). First of all, it is convenient to explore the winter mean turbulent heat flux provided by ERA-interim model, as it is the atmospheric forcing of the ocean reanalysis we here use (Fig. 12). As seen, the largest turbulent heat loss within the period 1988–2018 occurs in the Gulf of Lion during the winter of year 2005, with a minimum value below −1200 kJ m^{-2}. In terms of meridional overturning, we detect a dramatic increase of transport in density space in the WMED during winter of 2006 at around 41°N (Fig. 13, the region is indicated by a rectangle). Unsurprisingly, from winter depth anomalies of water masses with $\rho = 1029\,\mathrm{kg\ m^{-3}}$ (which are those water masses associated with the strong transport shown in Fig. 13), we observe that they are located about 100 m closer to the surface than on average (see Fig. 14, note also the notable isopycnal upward displacement during the strong convection event of winter 2012), even some of them emerging (compare against mean winter depth in Fig. S12), which is substantially more than in neighboring years. By distinguishing the winter mean impact on the overturning meridional transport in the WMED for selected water classes of potential density, potential temperature and salinity, we are able to verify that a strong anomalous transport occurred in winter of years 2005 and 2006 for

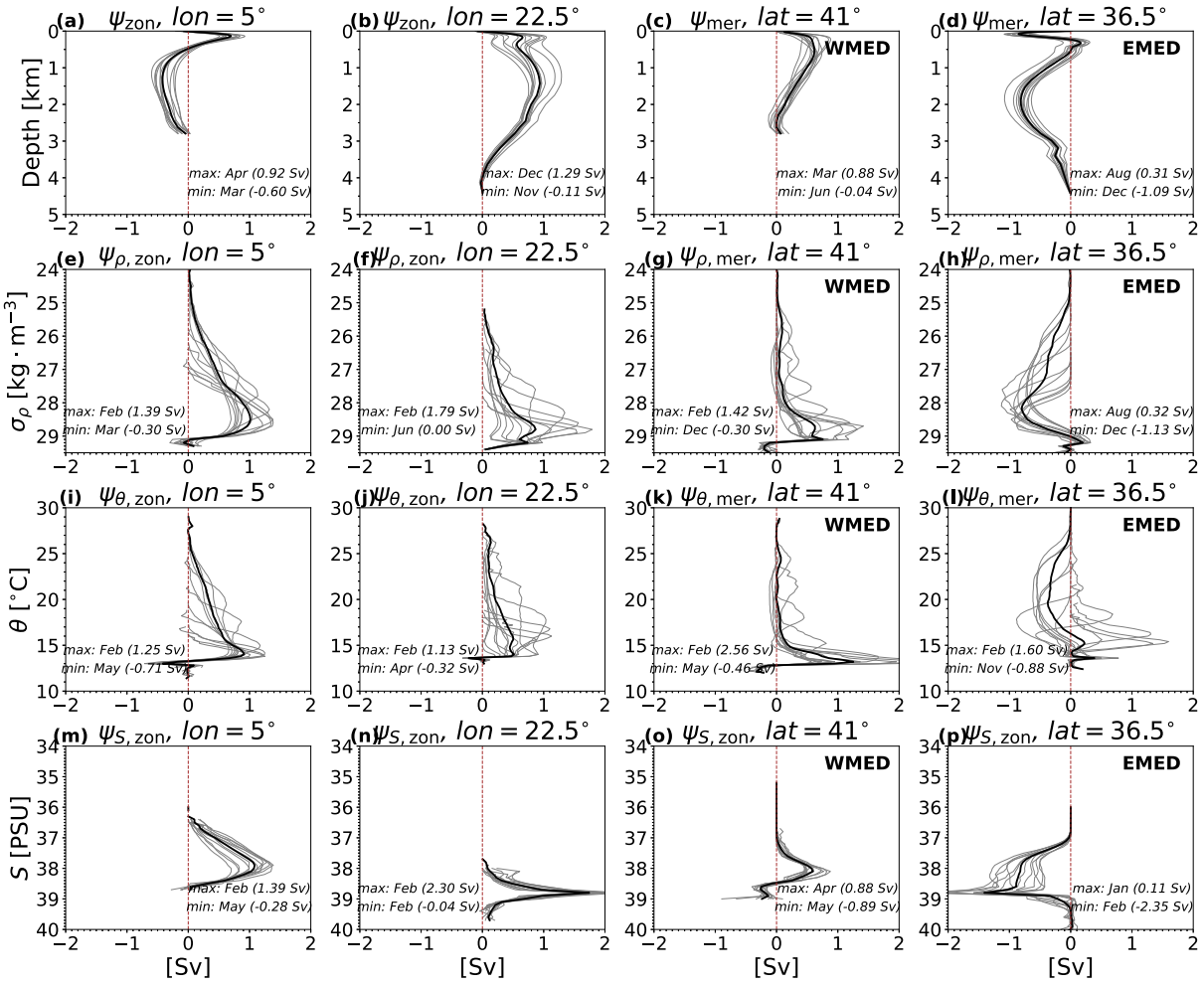

Fig. 9. Vertical profiles of mean zonal (first two columns) and meridional (last two columns) overturning transport at selected sections: (a)–(e)-(i)–(m) 5°E, (b)–(f)-(j)–(n) 22.5°E, (c)–(g)-(k)–(o) 41°N and (d)–(h)-(l)–(p) 36.5°N. Results are shown for: (a-d) depth space, (e-h) potential density anomalies (σ_ρ) space, (i-l) θ space and S space (m-p). The mean values (black lines) cover the period 1987–2018 (both included). Also the climatology (monthly mean profiles) are included as gray lines in each panel. Unit in Sv.

dense water masses of around $\rho = 1029\,\mathrm{kg\ m^{-3}}$, $S = 38$–38.5 and around $\theta = 13\,^{\circ}\mathrm{C}$, being this transport larger for water masses with these characteristics than in any other year (Fig. 15).

6. Discussion and conclusions

In this work we have employed a Mediterranean Sea reanalysis of monthly mean ocean currents to explore the ability of overturning metrics to detect and monitor seasonal and interannual changes in ocean circulation. This has been addressed not only by analyzing these changes at basin scale but also for smaller scale events such as atmospheric-induced winter deep convection episodes. By studying the seasonal and interannual overturning dynamics in terms of water mass properties (potential density, potential temperature and salinity), we complement the previous analysis performed by Pinardi et al. (2019) and Lyubartsev et al. (2020) in depth space.

Unsurprisingly, the mean zonal overturning reveals a strong clockwise cell in all three potential density, salinity and potential temperature spaces, which is more difficult to see in depth space as there appears a large counterclockwise cell in the WMED (below 500 m, Fig. 1b–c). This zonal overturning is largely controlled by salinity in the EMED (Fig. 3g), as expected from its strong evaporative character. The mean largest accumulated transport in salinity space (> 1.6 Sv) takes place between the Adriatic and the Aegean seas. Contrarily, a mean weak accumulated transport (< 0.5 Sv) is detected in θ space in the EMED (Fig. 3e). In contrast, overturning in the WMED is controlled by both, θ and S (Fig. 3e,g).

Interestingly, the meridional component of EMED overturning responds faster to changes in the circulation, as shown by the fact that the Eastern Mediterranean Transient was detected about 1 yr earlier in the EMED meridional component (1992, Fig. 4) than in the zonal one (1993, Fig. 3). Likely, this delay is mainly due to the fact that meridional cells are relatively weaker and smaller than zonal ones, therefore they are more sensitive to perturbations. Besides, to be further explored is the existence of a delay of 1 year between the maximum meridional transport in depth and density spaces in the EMED during the EMT (Fig. 11f).

Our results show that seasonal variations of overturning are noticeable in all spaces, being the dominant zonal cell, associated with surface and intermediate layers, substantially narrower in winter than in summer because of the large homogenization caused by winter cooling and mixing (Testor et al., 2018). This fact is reflected in a weakening of overturning during summer in both zonal and meridional components for all spaces (Figs. 6–8). Remarkably, during winter the

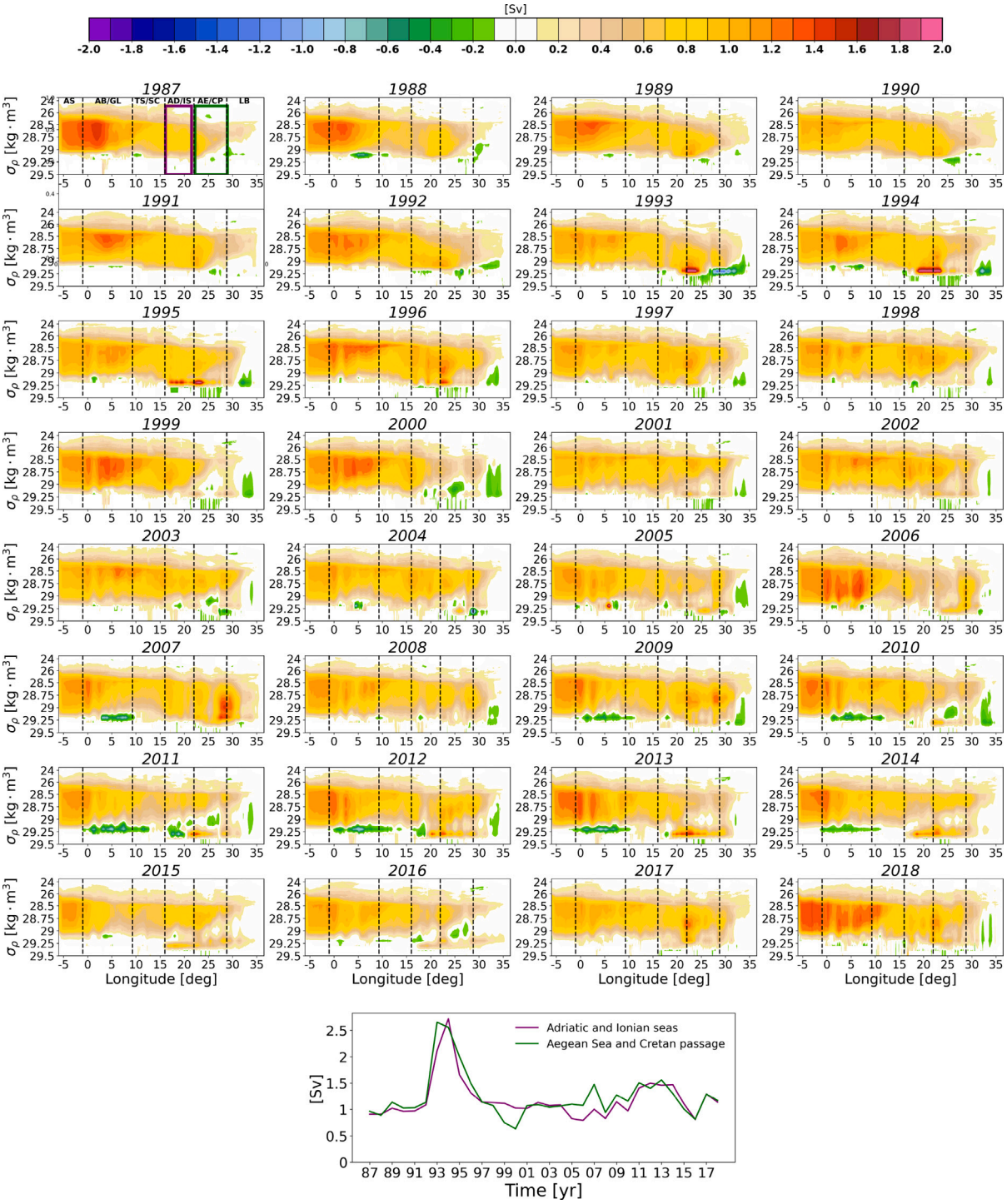

Fig. 10. Yearly mean zonal overturning in potential density anomalies (σ_ρ) space. Bottom panel: annual mean maximum transport in Adriatic and Ionian seas (purple rectangle) and Aegean Sea and Cretan Passage (green rectangle). Unit in Sv. Acronyms were defined in Fig. 3.

EMED upper meridional cell reverses its sense with respect to the rest of the seasons in potential temperature space (switching from counterclockwise to clockwise sense, see Figs. 8i, 9l). The latter is likely caused by the strong densification that takes place there during winter, mixing surface with intermediate water masses.

Regarding interannual variations of overturning, changes in the shape and values of annual mean overturning are observed in all water mass spaces (reaching values of up to 2 Sv, depending on the region considered, Fig. 10 and Fig. S2–S9). By restricting our analysis to winter time, when the Mediterranean Sea is more affected by the atmosphere, significant quasi-instantaneous correlations between the main Mediterranean Sea climate indices (Criado-Aldeanueva and Soto-Navarro, 2020) and overturning time series distinguished by basins are revealed. In particular, we note that, there exists a negative

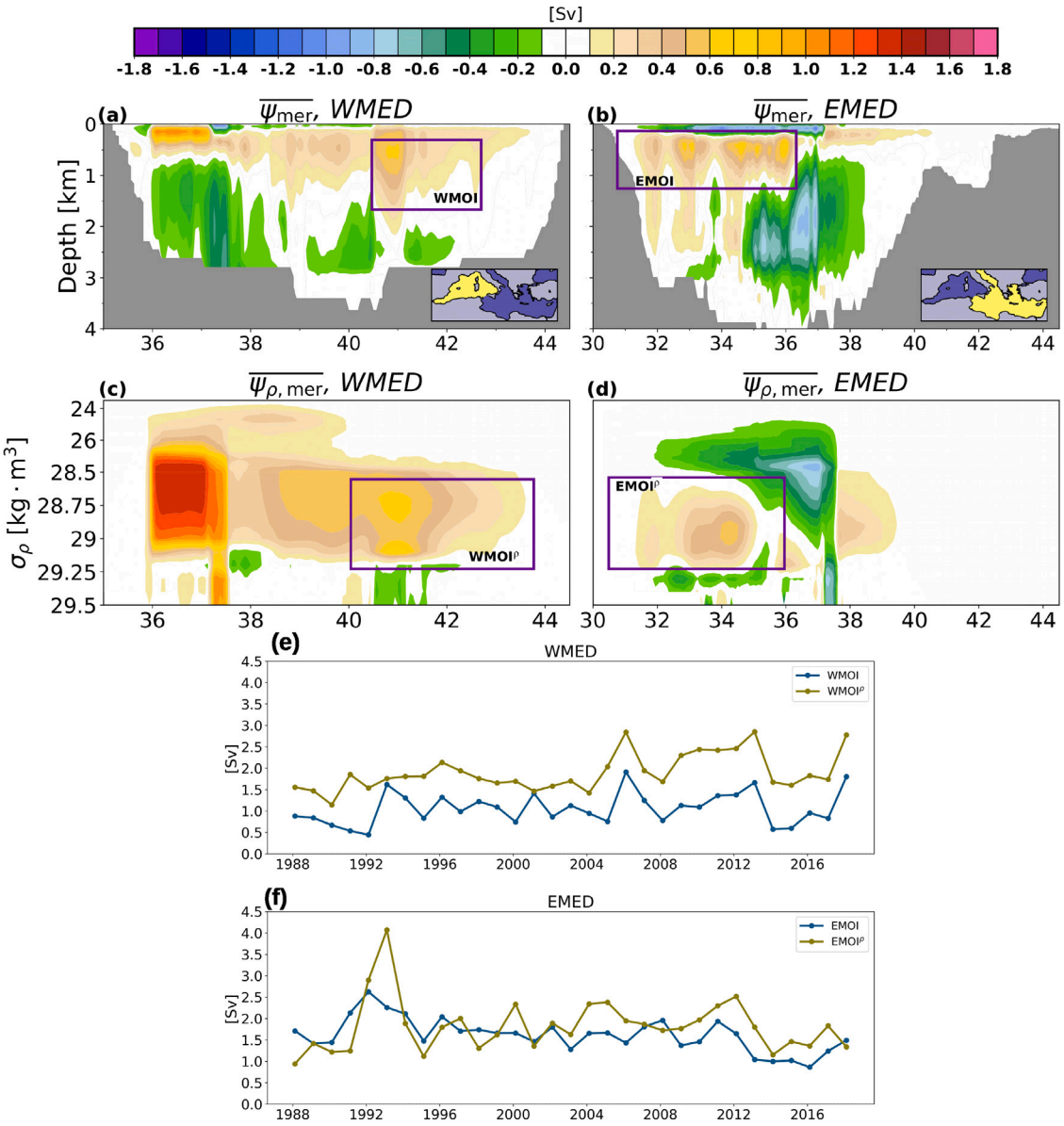

Fig. 11. Meridional overturning circulation between years 1987 and 2018 (both included) distinguishing for Western Mediterranean (WMED, panels (a)–(c)) and Eastern Mediterranean (EMED, panels (b)–(d)) sub-basins. Meridional transport is shown for: depth space (first row) and potential density anomalies space (second row). Regions where overturning indices are defined are depicted by a rectangle: WMOI (a), EMOI (b), WMOI$^{\rho}$ (c) and EMOI$^{\rho}$ (d). Time series of winter WMED overturning indices and EMED indices are displayed in panels (e) and (f), respectively. Unit in Sv.

correlation between the WMOI (associated with the northern clockwise meridional cell) in density space (WMOI$^{\rho}$) with respect to MOI$_1$, NAO and EA. It means that when winters are harsher (a negative NAO is linked to higher probability of passages of atmospheric perturbations) overturning gets stronger (Mellado-Cano et al., 2019). In contrast, this correlation is positive with the SCAND mode as during its positive phase winters are colder than usual (Table 1). In the EMED, the EMOI in density space (EMOI$^{\rho}$, associated with the clockwise cell) strengthens during the negative EA phase (colder winter than usual in the Mediterranean Sea) and during the positive EA-WR phase (Table 1), which is also associated with colder than usual winters in western Russia and northeastern Africa because of the intensification of northerlies in the EMED (Rogers, 1990). It is remarkable the fact that correlations are generally higher in density than in depth space.

Overturning metrics also yield interesting information on regional Mediterranean Sea dynamics at sub-basin scale, being able to detect strong changes at intermediate and deeper layers. A couple of selected examples that we have analyzed in this work are the Eastern Mediterranean Transient and the extraordinary winter deep convection events of 2004–2006 in the northwestern WMED, where the mixed layer reached depths below 2000 m in some locations and marked the beginning of the WMT (Smith et al., 2008; Schroeder et al., 2016). As shown in Fig. 10, overturning in potential density space is able to track the exceptional tongue of dense water masses formed in the Aegean Sea and around the Cretan Passage in 1993 that moved westward the following year. Hence, overturning constructed over water mass properties provides information on water mass flow and physical characteristics being thus potentially useful to monitor Mediterranean

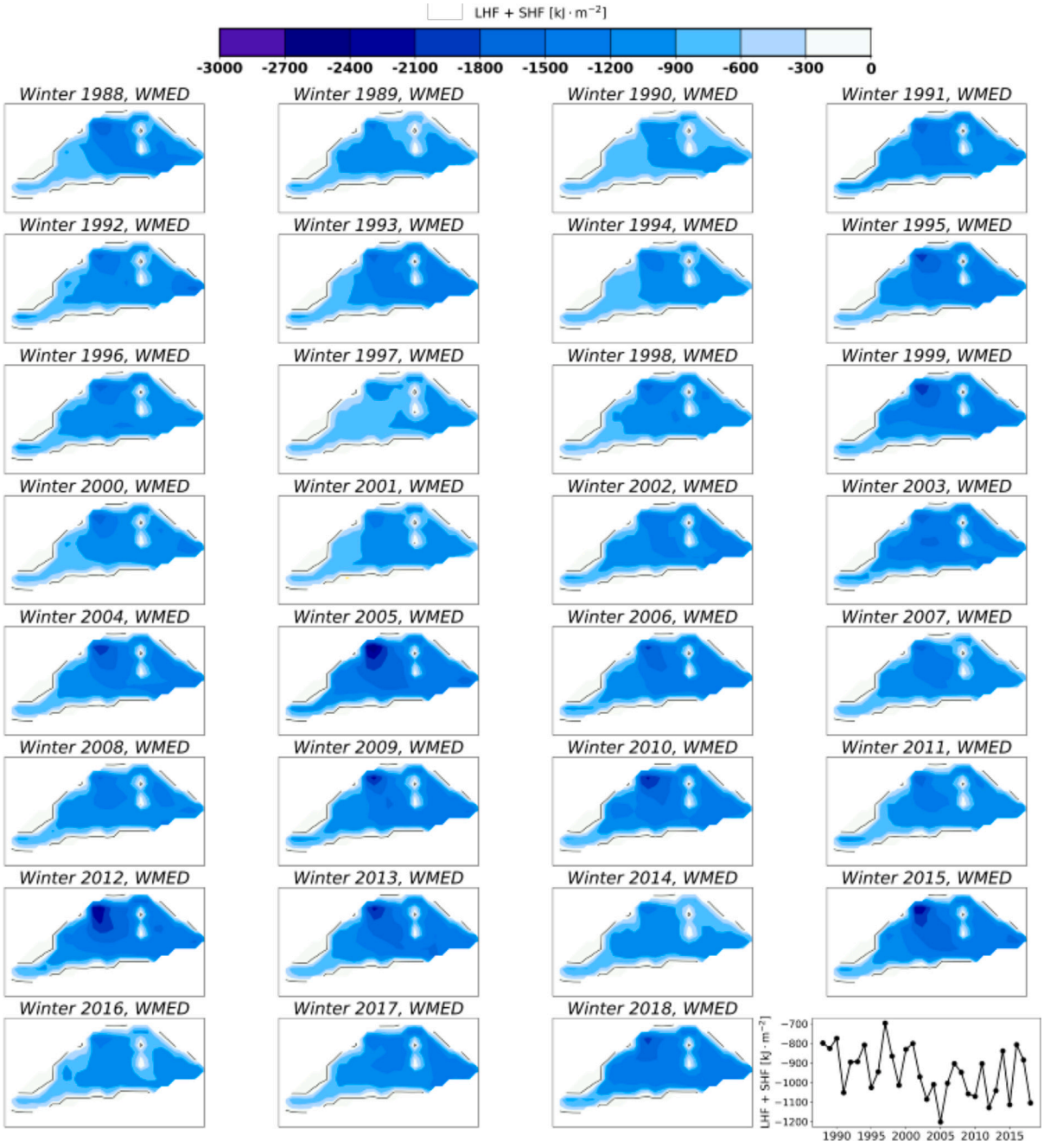

Fig. 12. Winter (December to March) mean surface turbulent heat flux (latent + sensible heat flux) derived from ERA-interim atmospheric reanalysis from 1988 to 2018 (both included). The bottom right panel shows the time series of WMED winter minimum total turbulent heat flux. Note that a negative sign indicates ocean heat loss. Unit in kJ m^{-2}.

Sea transport variations, and to identify those water masses ultimately responsible for those changes. Finally, it is worthy to stress that the long term monitoring of overturning in all spaces may provide early evidences of ongoing changes in the Mediterranean Sea circulation.

Declaration of competing interest

The authors declare that they have no known competing financial interests or personal relationships that could have appeared to influence the work reported in this paper.

Data availability

Data will be made available on request.

Acknowledgments

J.-M. Sayol thanks the financial support by Generalitat Valenciana, Spain and the European Social Fund (ESF) through the APOSTD/2020/254 grant. Part of this research was performed during his visit to IMEDEA (UIB-CSIC), also funded by the APOSTD/2020/254 grant. D. García-García and I. Vigo are partially funded by Spanish Ministry of Science, Innovation and Universities grant number PID2021-122142OB-I00, and Generalitat Valenciana, Spain grant numbers PROMETEO/2021/030 and GVA-THINKINAZUL/2021/035.

Appendix A. Supplementary data

Supplementary material related to this article can be found online at https://doi.org/10.1016/j.dsr.2023.104081.

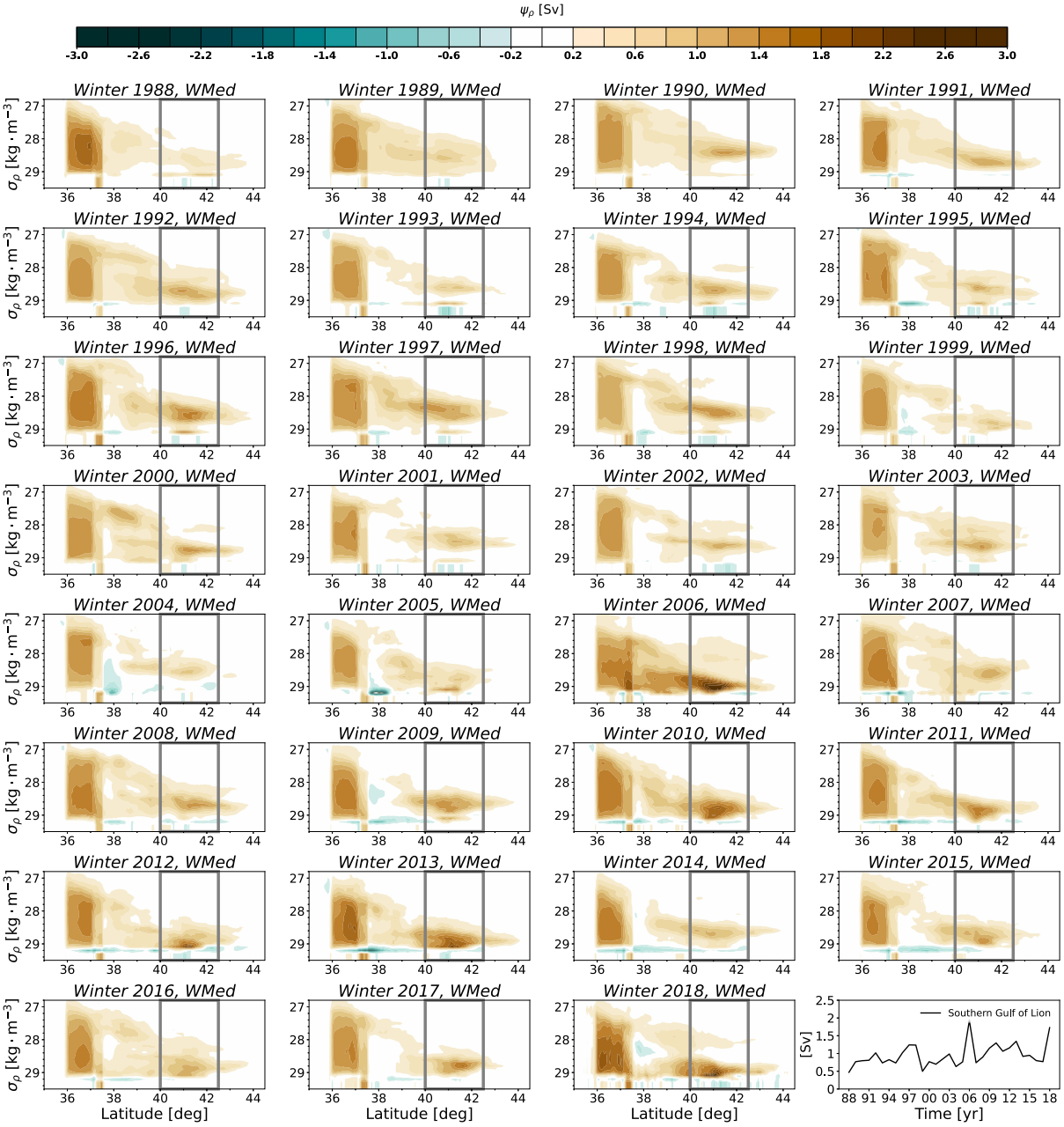

Fig. 13. Meridional winter mean overturning transport in potential density anomalies (σ_ρ) space in the WMED. Those latitudes associated with the Gulf of Lion are indicated by a rectangle. Unit in Sv. In the bottom right panel the time series of the mean of the monthly maximum overturning for the southern Gulf of Lion indicated in the rectangle is depicted.

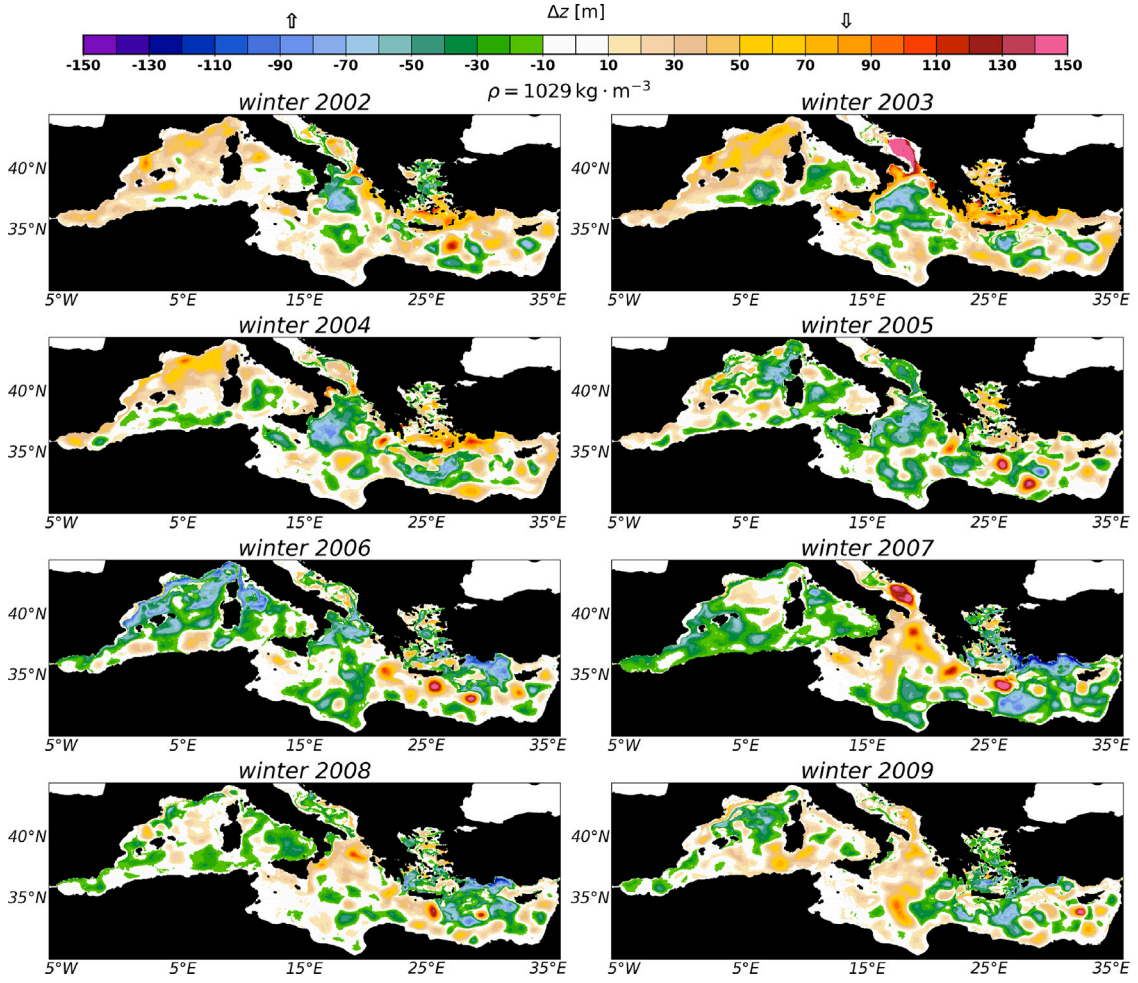

Fig. 14. Mean winter depth anomalies of those water masses with $\rho = 1029\,\mathrm{kg\ m^{-3}}$ from winter 2002 (i.e., December 2001 to March 2002) to winter 2009 with respect to the 1988–2018 winter climatology. Negative values mean water masses move upward, while positive values are related with downward displacements. Unit in m.

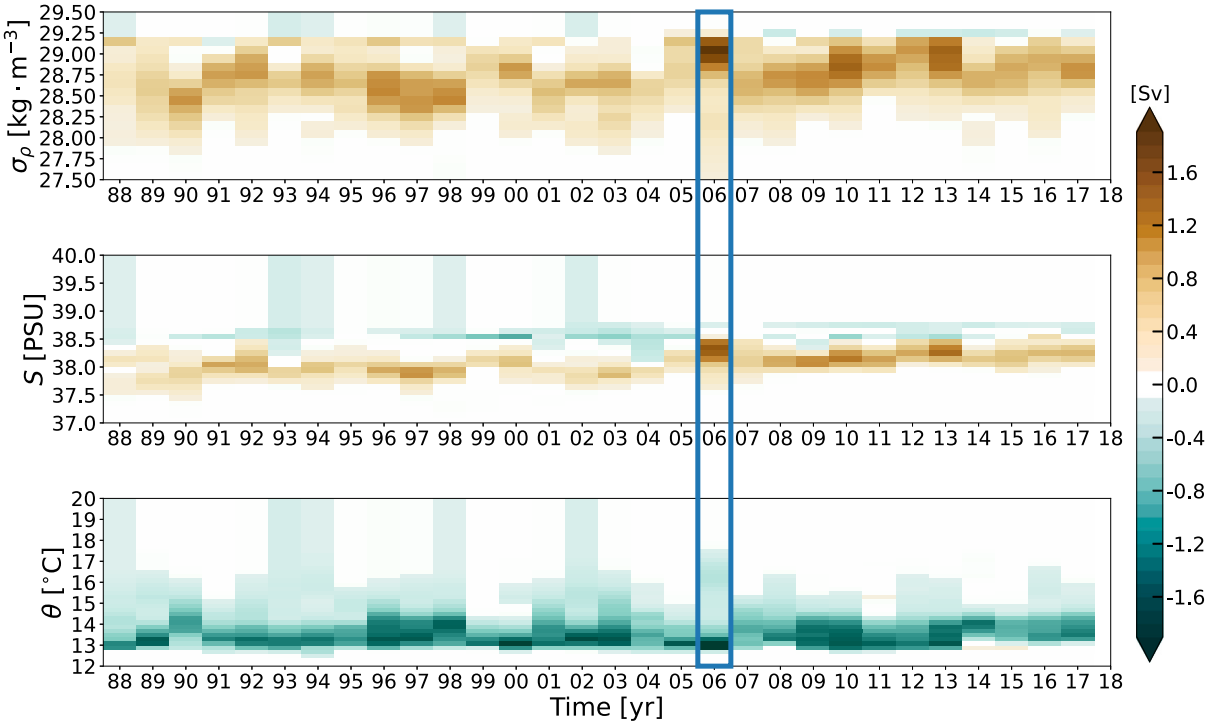

Fig. 15. Time series of winter mean meridional overturning transport in the WMED distinguished by water mass properties from winter of 1988 to winter of 2018 for potential density anomalies space (top panel), potential temperature space (middle panel), and salinity space (bottom panel). Unit in Sv.

References

Aldama-Campino, A., Döös, K., 2020. Mediterranean overflow water in the North Atlantic and its multidecadal variability. Tellus A 72 (1), 1–10. http://dx.doi.org/10.1080/16000870.2018.1565027.

Astraldi, M., Balopoulos, S., Candela, J., Font, J., Gacic, M., Gasparini, G., Manca, B., Theocharis, A., Tintoré, J., 1999. The role of straits and channels in understanding the characteristics of Mediterranean circulation. Prog. Oceanogr. 44 (1), 65–108. http://dx.doi.org/10.1016/S0079-6611(99)00021-X, URL: https://www.sciencedirect.com/science/article/pii/S007966119900021X.

Ayache, M., Swingedouw, D., Colin, C., Dutay, J.-C., 2021. Evaluating the impact of mediterranean overflow on the large-scale atlantic ocean circulation using neodymium isotopic composition. Palaeogeogr. Palaeoclimatol. Palaeoecol. 570, 110359. http://dx.doi.org/10.1016/j.palaeo.2021.110359, URL: https://www.sciencedirect.com/science/article/pii/S0031018221001449.

Barnston, A.G., Livezey, R.E., 1987. Classification, seasonality and persistence of low-frequency atmospheric circulation patterns. Mon. Weather Rev. 115 (6), 1083–1126. http://dx.doi.org/10.1175/1520-0493(1987)115<1083:CSAPOL>2.0.CO;2, URL: https://journals.ametsoc.org/view/journals/mwre/115/6/1520-0493_1987_115_1083_csapol_2_0_co_2.xml.

Bergamasco, A., Malanotte-Rizzoli, P., 2010. The circulation of the Mediterranean Sea: a historical review of experimental investigations. Adv. Oceanogr. Limnol. 1 (1), 11–28. http://dx.doi.org/10.1080/19475721.2010.491656.

Boers, N., 2021. Observation-based early-warning signals for a collapse of the atlantic meridional overturning circulation. Nature Clim. Change 11 (8), 680–688. http://dx.doi.org/10.1038/s41558-021-01097-4.

Bower, A., Lozier, S., Biastoch, A., Drouin, K., Foukal, N., Furey, H., Lankhorst, M., Rühs, S., Zou, S., 2019. Lagrangian views of the pathways of the Atlantic meridional overturning circulation. J. Geophys. Res.: Oceans 124 (8), 5313–5335. http://dx.doi.org/10.1029/2019JC015014, URL: https://agupubs.onlinelibrary.wiley.com/doi/abs/10.1029/2019JC015014.

Brüggemann, N., Katsman, C.A., 2019. Dynamics of downwelling in an eddying marginal sea: Contrasting the Eulerian and the isopycnal perspective. J. Phys. Oceanogr. 49 (11), 3017–3035. http://dx.doi.org/10.1175/JPO-D-19-0090.1.

Conte, M., Giuffrida, A., Tedesco, S., 1989. The Mediterranean Oscillation. Impact on Precipitation and Hydrology in Italy Climate Water. Technical Report, Publications of the Academy of Finland, Helsinki.

Criado-Aldeanueva, F., Soto-Navarro, J., 2020. Climatic indices over the Mediterranean Sea: A review. Appl. Sci. 10 (17), http://dx.doi.org/10.3390/app10175790, URL: https://www.mdpi.com/2076-3417/10/17/5790.

Dee, D., Coauthors, 2011. The ERA-interim reanalysis: Configuration and performance of the data assimilation system. Q. J. R. Meteorol. Soc. 137, 553–597. http://dx.doi.org/10.1002/qj.828.

Demirov, E.K., Pinardi, N., 2007. On the relationship between the water mass pathways and eddy variability in the Western Mediterranean Sea. J. Geophys. Res.: Oceans 112 (C2), http://dx.doi.org/10.1029/2005JC003174, URL: https://agupubs.onlinelibrary.wiley.com/doi/abs/10.1029/2005JC003174.

Dobricic, S., Pinardi, N., 2008. An oceanographic three- dimensional variational data assimilation scheme. Ocean Modell. 22, 89–105. http://dx.doi.org/10.1016/j.ocemod.2008.01.004.

Drijfhout, S., 2015. Competition between global warming and an abrupt collapse of the AMOC in Earth's energy imbalance. Sci. Rep. 5 (1), 14877. http://dx.doi.org/10.1038/srep14877.

Fofonoff, N., Millard, Jr., R., 1983. Algorithms for the Computation of Fundamental Properties of Seawater. Technical Report 44, UNESCO Technical Papers in Marine Sciences, Paris, France, p. 53. http://dx.doi.org/10.25607/OBP-1450.

Fox-Kemper, B., Hewitt, H., Xiao, C., Að algeirsdóttir, G., Drijfhout, S., Edwards, T., Golledge, N., Hemer, M., Kopp, R., Krinner, G., Mix, A., Notz, D., Nowicki, S., Nurhati, I., Ruiz, L., Sallée, J.-B., Slangen, A., Yu, Y., 2021. Ocean, cryosphere and sea level change. In: Masson-Delmotte, V., Zhai, P., Pirani, A., Connors, S., Péan, C., Berger, S., Caud, N., Chen, Y., Goldfarb, L., Gomis, M., Huang, M., Leitzell, K., Lonnoy, E., Matthews, J., Maycock, T., Waterfield, T., Yelekçi, O., Yu, R., Zhou, B. (Eds.), In Climate Change 2021: The Physical Science Basis. Contribution of Working Group I to the Sixth Assessment Report of the Intergovernmental Panel on Climate Change. Cambridge University Press, Cambridge, pp. 266–290

García-García, D., Vigo, I., Trottini, M., Vargas, J., Sayol, J., 2022. Hydrological cycle of the mediterranean-black sea system. Clim. Dynam. 59, 1919–1938. http://dx.doi.org/10.1007/s00382-022-06188-2.

Gascard, J.C., 1978. Mediterranean deep water formation barclonic instability and oceanic eddies. Oceanol. Acta. 1 (3), 315–330.

Georgiou, S., Ypma, S.L., Brüggemann, N., Sayol, J.-M., van der Boog, C.G., Spence, P., Pietrzak, J.D., Katsman, C.A., 2021. Direct and indirect pathways of convected water masses and their impacts on the overturning dynamics of the labrador sea. J. Geophys. Res.: Oceans 126 (1), http://dx.doi.org/10.1029/2020JC016654, e2020JC016654 2020JC016654, URL: https://agupubs.onlinelibrary.wiley.com/doi/abs/10.1029/2020JC016654.

Hainbucher, D., Rubino, A., Klein, B., 2006. Water mass characteristics in the deep layers of the western Ionian Basin observed during May 2003. Geophys. Res. Lett. 33 (5), http://dx.doi.org/10.1029/2005GL025318, URL: https://agupubs.onlinelibrary.wiley.com/doi/abs/10.1029/2005GL025318.

Heslop, E.E., Ruiz, S., Allen, J., López-Jurado, J.L., Renault, L., Tintoré, J., 2012. Autonomous underwater gliders monitoring variability at "choke points" in our ocean system: A case study in the Western Mediterranean Sea. Geophys. Res. Lett. 39 (20), http://dx.doi.org/10.1029/2012GL053717, URL: https://agupubs.onlinelibrary.wiley.com/doi/abs/10.1029/2012GL053717.

Houpert, L., Durrieu de Madron, X., Testor, P., Bosse, A., D'Ortenzio, F., Bouin, M.N., Dausse, D., Le Goff, H., Kunesch, S., Labaste, M., Coppola, L., Mortier, L., Raimbault, P., 2016. Observations of open-ocean deep convection in the northwestern Mediterranean Sea: Seasonal and interannual variability of mixing and deep water masses for the 2007–2013 Period. J. Geophys. Res.: Oceans 121 (11), 8139–8171. http://dx.doi.org/10.1002/2016JC011857, URL: https://agupubs.onlinelibrary.wiley.com/doi/abs/10.1002/2016JC011857.

Jackett, D.R., Mcdougall, T.J., 1995. Minimal adjustment of hydrographic profiles to achieve static stability. J. Atmos. Ocean. Technol. 12 (2), 381–389. http://dx.doi.org/10.1175/1520-0426(1995)012<0381:MAOHPT>2.0.CO;2, URL: https://journals.ametsoc.org/view/journals/atot/12/2/1520-0426_1995_012_0381_maohpt_2_0_co_2.xml.

Josey, S.A., 2003. Changes in the heat and freshwater forcing of the eastern Mediterranean and their influence on deep water formation. J. Geophys. Res.: Oceans 108 (C7), http://dx.doi.org/10.1029/2003JC001778, URL: https://agupubs.onlinelibrary.wiley.com/doi/abs/10.1029/2003JC001778.

Josey, S.A., Somot, S., Tsimplis, M., 2011. Impacts of atmospheric modes of variability on Mediterranean Sea surface heat exchange. J. Geophys. Res.: Oceans 116 (C2), http://dx.doi.org/10.1029/2010JC006685, URL: https://agupubs.onlinelibrary.wiley.com/doi/abs/10.1029/2010JC006685.

Katsman, C.A., Drijfhout, S.S., Dijkstra, H.A., Spall, M.A., 2018. Sinking of dense North Atlantic waters in a global ocean model: Location and controls. J. Geophys. Res.: Oceans 123 (5), 3563–3576. http://dx.doi.org/10.1029/2017JC013329, URL: https://agupubs.onlinelibrary.wiley.com/doi/abs/10.1029/2017JC013329.

Klein, B., Roether, W., Civitarese, G., Gacic, M., Manca, B.B., d'Alcala, M.R., 1999. Is the adriatic returning to dominate the production of Eastern Mediterranean Deep Water? Geophys. Res. Lett. 27 (20), 3377–3380. http://dx.doi.org/10.1029/2000GL011620, URL: https://agupubs.onlinelibrary.wiley.com/doi/abs/10.1029/2000GL011620.

Krichak, S.O., Alpert, P., 2005. Decadal trends in the east Atlantic–west Russia pattern and Mediterranean precipitation. Int. J. Climatol. 25 (2), 183–192. http://dx.doi.org/10.1002/joc.1124, URL: https://rmets.onlinelibrary.wiley.com/doi/abs/10.1002/joc.1124.

Lascaratos, A., Roether, W., Nittis, K., Klein, B., 1999. Recent changes in deep water formation and spreading in the eastern Mediterranean Sea: a review. Prog. Oceanogr. 44 (1), 5–36. http://dx.doi.org/10.1016/S0079-6611(99)00019-1, URL: https://www.sciencedirect.com/science/article/pii/S0079661199000191.

Liu, W., Fedorov, A.V., Xie, S.-P., Hu, S., 2020. Climate impacts of a weakened Atlantic Meridional Overturning Circulation in a warming climate. Sci. Adv. 6 (26), 4876. http://dx.doi.org/10.1126/sciadv.aaz4876, URL: https://www.science.org/doi/abs/10.1126/sciadv.aaz4876.

Lozier, M.S., Li, F., Bacon, S., Bahr, F., Bower, A.S., Cunningham, S.A., de Jong, M.F., de Steur, L., deYoung, B., Fischer, J., Gary, S.F., Greenan, B.J.W., Holliday, N.P., Houk, A., Houpert, L., Inall, M.E., Johns, W.E., Johnson, H.L., Johnson, C., Karstensen, J., Koman, G., Le Bras, I.A., Lin, X., Mackay, N., Marshall, D.P., Mercier, H., Oltmanns, M., Pickart, R.S., Ramsey, A.L., Rayner, D., Straneo, F., Thierry, V., Torres, D.J., Williams, R.G., Wilson, C., Yang, J., Yashayaev, I., Zhao, J., 2019. A sea change in our view of overturning in the subpolar North Atlantic. Science 363 (6426), 516–521. http://dx.doi.org/10.1126/science.aau6592, URL: https://science.sciencemag.org/content/363/6426/516.

Lyubartsev, V., Borile, F., Clementi, E., Masina, S., Drudi, M., Coppini, G., Cessi, P., Pinardi, N., 2020. Studying mobile context-aware social services in the wild. In: Copernicus Marine Service Ocean State Report, Issue 4. pp. s88–s91. http://dx.doi.org/10.1080/1755876X.2020.1785097, Journal of Operational Oceanography, 13:sup1.

Madec, G., 2008. NEMO Ocean Engine. Note du Pole de modelisation 27, Institut Pierre-Simon Laplace, p. 209.

Maillard, C., Coauthors, 2005. A Mediterranean and Black Sea oceanographic database and network. Boll. Geofis. Teor. Appl. 46 (4), 329–343.

Malanotte-Rizzoli, P., Manca, B.B., d'Alcala, M.R., Theocharis, A., Brenner, S., Budillon, G., Ozsoy, E., 1999. The Eastern Mediterranean in the 80s and in the 90s: the big transition in the intermediate and deep circulations. Dyn. Atmos. Oceans 29 (2), 365–395. http://dx.doi.org/10.1016/S0377-0265(99)00011-1, URL: https://www.sciencedirect.com/science/article/pii/S0377026599000111.

Manca, B.B., Ibello, V., Pacciaroni, M., Scarazzato, P., Giorgetti, A., 2006. Ventilation of deep waters in the Adriatic and Ionian seas following changes in thermohaline circulation of the Eastern Mediterranean. Clim. Res. 31 (2–3), 239–256. http://dx.doi.org/10.3354/cr031239, URL: https://www.int-res.com/abstracts/cr/v31/n2-3/p239-256/.

Margirier, F., Testor, P., Heslop, E., Mallil, K., Bosse, A., Houpert, L., Mortier, L., Bouin, M.-N., Coppola, L., D'Ortenzio, F., Durrieu de Madron, X., Mourre, B., Prieur, L., Raimbault, P., Taillandier, V., 2020. Abrupt warming and salinification of intermediate waters interplays with decline of deep convection in the Northwestern Mediterranean Sea. Sci. Rep. 10 (1), 20923. http://dx.doi.org/10.1038/s41598-020-77859-5.

Mauri, E., Sitz, L., Gerin, R., Poulain, P.-M., Hayes, D., Gildor, H., 2019. On the variability of the circulation and water mass properties in the Eastern Levantine Sea between September 2016–August 2017. Water 11 (9), http://dx.doi.org/10.3390/w11091741, URL: https://www.mdpi.com/2073-4441/11/9/1741.

Mellado-Cano, J., Barriopedro, D., García-Herrera, R., Trigo, R.M., Hernández, A., 2019. Examining the North Atlantic oscillation, East Atlantic pattern, and jet variability since 1685. J. Clim. 32 (19), 6285–6298. http://dx.doi.org/10.1175/JCLI-D-19-0135.1, URL: https://journals.ametsoc.org/view/journals/clim/32/19/jcli-d-19-0135.1.xml.

Menna, M., Gerin, R., Notarstefano, G., Mauri, E., Bussani, A., Pacciaroni, M., Poulain, P.-M., 2021. On the circulation and thermohaline properties of the Eastern Mediterranean Sea. Front. Mar. Sci. 8, 903. http://dx.doi.org/10.3389/fmars.2021.671469, URL: https://www.frontiersin.org/article/10.3389/fmars.2021.671469.

Millot, C., 1999. Circulation in the Western Mediterranean Sea. J. Mar. Syst. 20 (1), 423–442. http://dx.doi.org/10.1016/S0924-7963(98)00078-5, URL: https://www.sciencedirect.com/science/article/pii/S0924796398000785.

Millot, C., Gerin, R., 2010. The Mid-Mediterranean Jet Artefact. Geophys. Res. Lett. 37 (12), http://dx.doi.org/10.1029/2010GL043359, URL: https://agupubs.onlinelibrary.wiley.com/doi/abs/10.1029/2010GL043359.

Millot, C., Taupier-Letage, I., 2005. Circulation in the Mediterranean Sea. In: The Mediterranean Sea. Springer Berlin Heidelberg, Berlin, Heidelberg, pp. 29–66. http://dx.doi.org/10.1007/b107143.

Morales-Márquez, V., Orfila, A., Simarro, G., Marcos, M., 2020. Extreme waves and climatic patterns of variability in the eastern North Atlantic and Mediterranean basins. Ocean Sci. 16 (6), 1385–1398. http://dx.doi.org/10.5194/os-16-1385-2020, URL: https://os.copernicus.org/articles/16/1385/2020/.

Noaa, C., 2008. Teleconnection indices calculation procedures. http://www.cpc.ncep.noaa.gov/data/teledoc/teleindcalc.shtml. (Online accessed 19 September 2021).

Palutikof, J.P., 2003. Analysis of Mediterranean climate data: measured and modelled. In: Bolle, H.J. (Ed.), Mediterranean Climate: Variability and Trends. Springer-Verlag, Berlin.

Palutikof, J.P., Conte, M., Casimiro Mendes, J., Goodess, C.M., Espirito Santo, F., 1996. Mediterranean desertification and land use. In: Brandt, C.J., Thornes, J.B. (Eds.), Climate and Climate Change. John Wiley and Sons, London.

Pinardi, N., Cessi, P., Borile, F., Wolfe, C.L.P., 2019. The Mediterranean Sea overturning circulation. J. Phys. Oceanogr. 49 (7), 1699–1721. http://dx.doi.org/10.1175/JPO-D-18-0254.1, URL: https://journals.ametsoc.org/view/journals/phoc/49/7/jpo-d-18-0254.1.xml.

Pisacane, G., Artale, V., Calmanti, S., Rupolo, V., 2006. Decadal oscillations in the Mediterranean Sea: a result of the overturning circulation variability in the eastern basin? Clim. Res. 31 (2–3), 257–271. http://dx.doi.org/10.3354/cr031257, URL: https://www.int-res.com/abstracts/cr/v31/n2-3/p257-271/.

Rhein, M., 1995. Deep water formation in the western Mediterranean. J. Geophys. Res.: Oceans 100 (C4), 6943–6959. http://dx.doi.org/10.1029/94JC03198, URL: https://agupubs.onlinelibrary.wiley.com/doi/abs/10.1029/94JC03198.

Rixen, M., Beckers, J.-M., Levitus, S., Antonov, J., Boyer, T., Maillard, C., Fichaut, M., Balopoulos, E., Iona, S., Dooley, H., Garcia, M.-J., Manca, B., Giorgetti, A., Manzella, G., Mikhailov, N., Pinardi, N., Zavatarelli, M., 2005. The Western Mediterranean Deep Water: A proxy for climate change. Geophys. Res. Lett. 32 (12), http://dx.doi.org/10.1029/2005GL022702, URL: https://agupubs.onlinelibrary.wiley.com/doi/abs/10.1029/2005GL022702.

Roether, W., Manca, B.B., Klein, B., Bregant, D., Georgopoulos, D., Beitzel, V., Kovačević, V., Luchetta, A., 1996. Recent changes in Eastern Mediterranean Deep Waters. Science 271 (5247), 333–335, URL: http://www.jstor.org/stable/2890461, Full publication date: Jan. 19, 1996.

Rogers, J.C., 1990. Patterns of low-frequency monthly sea level pressure variability (1899–1986) and associated wave cyclone frequencies. J. Clim. 3 (12), 1364–1379. http://dx.doi.org/10.1175/1520-0442(1990)003<1364:POLFMS>2.0.CO;2, URL: https://journals.ametsoc.org/view/journals/clim/3/12/1520-0442_1990_003_1364_polfms_2_0_co_2.xml.

Rohling, E.J., Bryden, H.L., 1992. Man-induced salinity and temperature increases in western Mediterranean deep water. J. Geophys. Res.: Oceans 97 (C7), 11191–11198. http://dx.doi.org/10.1029/92JC00767, URL: https://agupubs.onlinelibrary.wiley.com/doi/abs/10.1029/92JC00767.

Sayol, J.-M., Dijkstra, H., Katsman, C., 2019. Seasonal and regional variations of sinking in the subpolar North Atlantic from a high-resolution ocean model. Ocean Sci. 15 (4), 1033–1053. http://dx.doi.org/10.5194/os-15-1033-2019, URL: https://os.copernicus.org/articles/15/1033/2019/.

Schröder, K., Gasparini, G.P., Tangherlini, M., Astraldi, M., 2006. Deep and intermediate water in the western mediterranean under the influence of the Eastern Mediterranean Transient. Geophys. Res. Lett. 33 (21), http://dx.doi.org/10.1029/2006GL027121, URL: https://agupubs.onlinelibrary.wiley.com/doi/abs/10.1029/2006GL027121.

Schroeder, K., Borghini, M., Cerrati, G., Difesca, V., Delfanti, R., Santinelli, C., Gasparini, G.P., 2008. Multiparametric mixing analysis of the deep waters in the Western Mediterranean Sea. Chem. Ecol. 24 (sup1), 47–56. http://dx.doi.org/10.1080/02757540801970373.

Schroeder, K., Chiggiato, J., Bryden, H.L., Borghini, M., Ben Ismail, S., 2016. Abrupt climate shift in the Western Mediterranean Sea. Sci. Rep. 6 (1), 23009. http://dx.doi.org/10.1038/srep23009.

Simoncelli, S., Fratianni, C., Pinardi, N., Grandi, A., Drudi, M., Oddo, P., Dobricic, S., 2017. Mediterranean sea physical reanalysis (MEDREA 1987–2015). Copernicus Monit. Environ. Mar. Serv. http://dx.doi.org/10.25423/medsea_reanalysis_phys_006_004.

Smeed, D.A., Josey, S.A., Beaulieu, C., Johns, W.E., Moat, B.I., Frajka-Williams, E., Rayner, D., Meinen, C.S., Baringer, M.O., Bryden, H.L., McCarthy, G.D., 2018. The North Atlantic Ocean is in a state of reduced overturning. Geophys. Res. Lett. 45 (3), 1527–1533. http://dx.doi.org/10.1002/2017GL076350, URL: https://agupubs.onlinelibrary.wiley.com/doi/abs/10.1002/2017GL076350.

Smeed, D.A., McCarthy, G.D., Cunningham, S.A., Frajka-Williams, E., Rayner, D., Johns, W.E., Meinen, C.S., Baringer, M.O., Moat, B.I., Duchez, A., Bryden, H.L., 2014. Observed decline of the Atlantic meridional overturning circulation 2004–2012. Ocean Sci. 10 (1), 29–38. http://dx.doi.org/10.5194/os-10-29-2014, URL: https://os.copernicus.org/articles/10/29/2014/.

Smith, R.O., Bryden, H.L., Stansfield, K., 2008. Observations of new western Mediterranean deep water formation using argo floats. Ocean Sci. 4 (2), 133–149. http://dx.doi.org/10.5194/os-4-133-2008, URL: https://os.copernicus.org/articles/4/133/2008/.

Testor, P., Bosse, A., Houpert, L., Margirier, F., Mortier, L., Legoff, H., Dausse, D., Labaste, M., Karstensen, J., Hayes, D., Olita, A., Ribotti, A., Schroeder, K., Chiggiato, J., Onken, R., Heslop, E., Mourre, B., D'ortenzio, F., Mayot, N., Lavigne, H., de Fommervault, O., Coppola, L., Prieur, L., Taillandier, V., Durrieu de Madron, X., Bourrin, F., Many, G., Damien, P., Estournel, C., Marsaleix, P., Taupier-Letage, I., Raimbault, P., Waldman, R., Bouin, M.-N., Giordani, H., Caniaux, G., Somot, S., Ducrocq, V., Conan, P., 2018. Multiscale observations of deep convection in the Northwestern Mediterranean Sea during winter 2012–2013 using multiple platforms. J. Geophys. Res.: Oceans 123 (3), 1745–1776. http://dx.doi.org/10.1002/2016JC012671, URL: https://agupubs.onlinelibrary.wiley.com/doi/abs/10.1002/2016JC012671.

Theocharis, A., Nittis, K., Kontoyiannis, H., Papageorgiou, E., Balopoulos, E., 1999. Climatic changes in the Aegean Sea influence the eastern Mediterranean thermohaline circulation (1986–1997). Geophys. Res. Lett. 26 (11), 1617–1620. http://dx.doi.org/10.1029/1999GL900320, URL: https://agupubs.onlinelibrary.wiley.com/doi/abs/10.1029/1999GL900320.

Vigo, M., Sánchez-Reales, J., Trottini, M., Chao, B., 2011. Mediterranean Sea level variations: Analysis of the satellite altimetric data, 1992–2008. J. Geodyn. 52 (3), 271–278. http://dx.doi.org/10.1016/j.jog.2011.02.002, URL: https://www.sciencedirect.com/science/article/pii/S0264370711000299.

Waldman, R., Brüggemann, N., Bosse, A., Spall, M., Somot, S., Sevault, F., 2018. Overturning the Mediterranean thermohaline circulation. Geophys. Res. Lett. 45 (16), 8407–8415. http://dx.doi.org/10.1029/2018GL078502, URL: https://agupubs.onlinelibrary.wiley.com/doi/abs/10.1029/2018GL078502.

Wu, P., Haines, K., Pinardi, N., 2000. Toward an understanding of deep-water renewal in the Eastern Mediterranean. J. Phys. Oceanogr. 30 (2), 443–458. http://dx.doi.org/10.1175/1520-0485(2000)030<0443:TAUODW>2.0.CO;2, URL: https://journals.ametsoc.org/view/journals/phoc/30/2/1520-0485_2000_030_0443_tauodw_2.0.co_2.xml.

Wüst, G., 1961. On the vertical circulation of the Mediterranean Sea. J. Geophys. Res. (1896-1977) 66 (10), 3261–3271. http://dx.doi.org/10.1029/JZ066i010p03261, URL: https://agupubs.onlinelibrary.wiley.com/doi/abs/10.1029/JZ066i010p03261.

Xie, P., Arkin, P., 1997. Global precipitation: A 17-year monthly analysis based on gauge observations, satellite estimates, and numerical model outputs. Bull. Am. Meteorol. Soc. 78, 2539–2558. http://dx.doi.org/10.1175/1520-0477(1997)078,2539:GPAYMA.2.0.CO;2.

Zavatarelli, M., Mellor, G.L., 1995. A numerical study of the Mediterranean Sea circulation. J. Phys. Oceanogr. 25 (6), 1384–1414. http://dx.doi.org/10.1175/1520-0485(1995)025<1384:ANSOTM>2.0.CO;2, URL: https://journals.ametsoc.org/view/journals/phoc/25/6/1520-0485_1995_025_1384_ansotm_2_0_co_2.xml.

Zhu, J., Liu, Z., Zhang, J., Liu, W., 2015. AMOC response to global warming: dependence on the background climate and response timescale. Clim. Dynam. 44 (11), 3449–3468. http://dx.doi.org/10.1007/s00382-014-2165-x.

Zika, J.D., England, M.H., Sijp, W.P., 2012. The ocean circulation in thermohaline coordinates. J. Phys. Oceanogr. 42 (5), 708–724. http://dx.doi.org/10.1175/JPO-D-11-0139.1, URL: https://journals.ametsoc.org/view/journals/phoc/42/5/jpo-d-11-0139.1.xml.

Zunino, P., Schroeder, K., Vargas-Yanez, M., Gasparini, G.P., Coppola, L., Garcia-Martinez, M.C., Moya-Ruiz, F., 2012. Effects of the Western Mediterranean Transition on the resident water masses: Pure warming, pure freshening and pure heaving. J. Mar. Syst. 96–97, 15–23. http://dx.doi.org/10.1016/j.jmarsys.2012.01.011, URL: https://hal.science/hal-03502661.